A New Experiment Run Group Proposal Submitted to Jefferson Lab PAC44

A Search for Hybrid Baryons in Hall B with CLAS12

Volker Burkert *(Contact Person, Spekesperson)*, Daniel S. Carman, Valery Kubarovsky, Victor Mokeev *(Spokesperson)*, Maurizio Ungaro, Veronique Ziegler
Thomas Jefferson National Accelerator Facility, Newport News, Virginia 23606, USA

Annalisa D'Angelo *(Spokesperson)*, Lucilla Lanza, Alessandro Rizzo
Università di Roma Tor Vergata and INFN Roma Tor Vergata, 00133 Rome, Italy

Gleb Fedotov, Boris Ishkhanov, Evgeny Isupov, Evgeny Golovach *(Spokesperson)*
Skobeltsyn Institute of Physics, Moscow State University, 119234 Moscow, Russia

Ralf Gothe *(Spokesperson)*, Iuliia Skorodumina
University of South Carolina, Columbia, South Carolina 29208, USA

Vincent Mathieu[†], Vladyslav Pauk, Alessandro Pilloni, Adam Szczepaniak[†]
Theory Center, Jefferson Laboratory, Newport News, Virginia 23606, USA
([†]*Joint with Indiana University, Bloomington, Indiana 47405, USA*)

Simon Capstick, Volker Crede
Florida State University, Tallahassee, Florida 32306, USA

Jan Ryckebushch
Ghent University, B-9000 Ghent, Belgium

Michael Döring
The George Washington University, Washington, DC 20052, USA

Philip Cole
Idaho State University, Pocatello, Idaho 83209, USA

Vincenzo Bellini, Francesco Mammoliti, Giuseppe Russo, Concetta Sutera, Francesco Tortorici
INFN, Sezione di Catania, 95125 Catania, Italy

Ilaria Balossino, Luca Barion, Giuseppe Ciullo, Marco Contalbrigo, Paola Lenisa, Aram Movsisyan, Luciano Pappalardo, Mateo Turisini
INFN, Sezione di Ferrara, 44100 Ferrara, Italy

Marco Battaglieri, Andrea Celentano, Raffaella De Vita, Erica Fanchini, Mikhail Osipenko, Marco Ripani, Elena Santopinto, Mauro Taiuti
INFN, Sezione di Genova, 16146 Genova, Italy

Alessandra Filippi
INFN, Sezione di Torino, 10125 Torino, Italy

César Fernández-Ramírez
Universidad Nacional Autónoma de México, 04510 Mexico City, Mexico

Inna Aznauryan
Yerevan Physics Institute, 375036 Yerevan, Armenia

and the CLAS Collaboration

Abstract

This Proposal aims to establish a program to search for new excited baryon states in the mass range from 1.8 GeV to 3 GeV, as well as to explore for the first time the behavior of resonance electrocouplings over the full spectrum of excited proton states at photon virtualities Q^2 approaching the photon point ($Q^2 < 0.2$ GeV^2). This work focuses on measuring $K^+\Lambda$, $K^+\Sigma^0$, and $\pi^+\pi^-p$ exclusive final states in CLAS12 and detecting the scattered electrons in the angular range from 2.5° to 35° using the electron detection capabilities of the Forward Tagger and the CLAS12 detector. The experiment will use longitudinally polarized electron beams of 6.6 GeV and 8.8 GeV to cover the range of invariant mass W up to 3 GeV and Q^2 from 0.05 GeV^2 to 2 GeV^2. The main aspects of the Proposal are to:

- search for new hybrid baryon states with the glue as an extra constituent component beyond the three constituent quarks by focusing measurements at $Q^2 < 1.0$ GeV^2 where the expected magnitudes of the hybrid electroexcitation amplitudes are maximal;

- search for three-quark "missing" resonances in the electroproduction of different hadronic final states with the highest fluxes of virtual photons ever achieved in exclusive meson electroproduction experiments;

- study the structure of prominent nucleon resonances in the mass range up to 3 GeV in the regime of large meson-baryon cloud contributions and explore the N^* longitudinal electroexcitation approaching the photon point.

Exclusive events from KY and $\pi^+\pi^-p$ final states will be selected and the unpolarized differential cross sections will be obtained, complemented by measurements of the differential transverse-transverse and transverse-longitudinal interference cross sections. From these data the $\gamma_v pN^*$ electrocouplings will be determined for all possible new states with I=1/2 and I=3/2 and with all possible J^P quantum numbers, and the Q^2 evolution of their helicity amplitudes will then be determined in the low Q^2 range ($Q^2 < 2$ GeV^2) for different reaction channels.

The hybrid baryons will be identified as additional states in the N^*-spectrum beyond the regular three-quark states. Since spin-parities of hybrid baryons are expected to be the same as those for regular three-quark states, the signature of the hybrid-baryon will emerge from the distinctively different low Q^2-evolution of the hybrid-baryon electrocouplings, due to the additional gluonic component in their wave function.

This kinematic range also corresponds to the largest contributions from the meson-baryon cloud, allowing us to improve our knowledge on this component, which is relevant to understand the structure of all N^* states studied so far [2, 3], as well as to explore the longitudinal N^* electroexcitations as the photon virtuality goes to zero. This program adds an important new physics component to the existing CLAS12 N^* program at 11 GeV, which aims to measure the transition form factors for all prominent N^* states up to the highest photon virtualities ever probed in exclusive reactions $Q^2 < 12$ GeV^2. The study of the spectrum and structure of excited nucleon states at distance scales from low to high Q^2, encompassing the regime where low-energy meson-baryon degrees of freedom dominate to the regime where quark degrees of freedom dominate, allows for the opportunity to better understand how the strong interaction of dressed quarks and gluons gives rise to the spectrum and structure of excited nucleon states and how these states emerge from QCD.

Contents

1 Introduction

The ongoing program at Jefferson Lab and several other laboratories to study the excitation of nucleons in the so-called nucleon resonance region with real photon and with electron beams has been very successful. Although only a fraction of the data taken during the CLAS run groups g8, g9, g11, and g12 have been analyzed and published, the published data have allowed for very significant advances in light-quark baryon spectroscopy, and led to strong evidence of several new nucleon excitations as listed in the PDG review of 2014 [1]. These discoveries were possible due to the very high meson production rates recently obtained for energy-tagged photoproduction processes. Furthermore, the use of meson electroproduction has led to completely new insights into the nature of several prominent resonant baryons, e.g. the so-called Roper resonance $N(1440)\frac{1}{2}^+$. This state defied an explanation of its properties, such as mass, transition amplitudes, and transition form factors within the constituent quark model (CQM). The analyses of the new electroproduction data were crucial in dissecting its complex structure and providing a qualitative and quantitative explanation of the space-time evolution of the state [4]. The Roper was also considered as a candidate for the lowest mass hybrid baryon [5]. It was only through the meson electroproduction data that this possibility could be dismissed [2, 6].

The theory of the strong interactions, QCD, not only allows for the existence of baryons with dominant gluonic contributions (hybrid baryons), but Lattice QCD calculations now predict several baryon states with dominant gluonic admixture to the wave function, and with the lowest mass hybrids approximately 1.3 GeV above the nucleon ground state of 0.94 GeV [7], i.e. in the range $W = 2.2 - 2.3$ GeV. In the meson sector, exotic states (hybrid mesons) are predicted with quantum numbers that cannot be obtained in a pure $q\bar{q}$ configuration. The selection of mesons with such exotic quantum numbers provides a convenient way to identify candidates for gluonic mesons. In contrast to the meson sector hybrid baryons have quantum numbers that are also populated by ordinary excited 3-quark states. Hybrid baryons hence mix with these 3-quark excited states or with dynamically generated states making the identification of gluonic baryons more difficult. An important question is therefore: How can we distinguish gluonic excitations of baryons from their ordinary quark excitations? Another question is the mass range in which we may expect hybrid baryons to occur.

Mapping out the nucleon spectrum and the excitation strengths of individual resonances is a powerful way to answer a central question of hadron physics: "What are the effective degrees of freedom as the excited states are probed at different distance scales?". Previous analyses of meson electroproduction have shown to be most effective in providing answers in several cases of excited states: $\Delta(1232)\frac{3}{2}^+$, $N(1440)\frac{1}{2}^+$, $N(1520)\frac{3}{2}^-$, $N(1535)\frac{1}{2}^-$, $N(1680)\frac{5}{2}^+$, and $N(1675)\frac{5}{2}^-$.

The experimental program outlined in this Proposal is meant to vastly improve upon the available information and extend the reach of meson electroproduction to cover the full nucleon resonance mass range up to 3 GeV and a larger low Q^2 range from 0.05 to 2 GeV^2, using electron beam energies of 6.6 GeV and 8.8 GeV. The unpolarized differential cross sections will be mesured for KY and $\pi^+\pi^-p$ exclusive channels, complemented by measurements of the differential transverse-transverse and transverse-longitudinal interference cross sections.

From these data the $\gamma_v pN^*$ electrocouplings will be determined employing the well known unitary isobar models and dispersion relation approaches that have proven very effective for the study of two-body final states such as πN [2, 8] and KY [9], as well as the Jlab-Moskov (JM) meson-baryon reaction model for $\pi^+\pi^- p$ electroproduction [3, 8], multi-channel partial wave techniques employing both the Bonn-Gatchina [10] and GWU [11] approaches, and approaches starting from the Veneziano model and Regge phenomenology [12] that are applicable at higher energies where many hadron channels open in the final state interactions.

The program will search for all possible new states with I=1/2 and I=3/2 and with all possible J^P quantum numbers. As new states are identified using the high event rates at very small Q^2 values ("quasi-real" photoproduction), the Q^2 dependence of their helicity amplitudes will be determined. The results at different values of Q^2 from the different exclusive channels will substantially enhance our capability for the discovery of new baryon states. Consistent results on resonance masses and $\gamma_v pN^*$ electrocouplings from the different exclusive decay channels, as well as Q^2-independent partial hadronic decay widths over the full Q^2-range, will offer convincing evidence for the existence of new states and the reliable extraction of their parameters. This approach has been highly effective in determining the Q^2 dependence of the $A_{1/2}$, $A_{3/2}$, and $S_{1/2}$ helicity amplitudes for several of the lower mass baryons, such as the $\Delta(1232)3/2^+$, the $N(1440)1/2^+$ and the $N(1535)1/2^-$ [2, 3]. These any many other results are included in the review of the N^* and Δ^* states in the latest edition of the PDG [13].

The hybrid baryons will be identified as additional states in the N^*-spectrum beyond the regular three-quark states as was predicted in recent LQCD studies of the baryon spectrum [7]. Since spin-parities of hybrid baryons are expected to be the same as those for regular three-quark states, information on the $\gamma_v pN^*$ electrocoupling evolution with Q^2 becomes critical in the search for hybrid baryons. A distinctively different Q^2-evolution of the hybrid-baryon electrocouplings is expected considering the different color-multiplet assignments for the quark-core in a regular versus a hybrid baryon, i.e. a color singlet and octet, respectively. Low photon virtualities offer a preferential regime for the studies of hybrid-baryon electrocouplings.

In conjunction with experiment E12-09-003, which focusses on the highest Q^2, as well as E12-06-108A, which explores $K^+\Lambda$ production, the proposed experiment will provide a complete program of nucleon resonance electroexcitation.

2 Theoretical Studies of Hybrid Baryons

2.1 Model projections

In an extension of the MIT bag model, gluonic excitations of the nucleon, to states where a constituent gluon in the lowest energy transverse electric mode combines with three quarks in a color octet state to form a colorless state in the mass range of 1.600 ± 0.100 GeV, have been broadly discussed since 1983 [5].

The gluon flux-tube model applied to hybrid baryons [14, 15] came up with similar quantum numbers of the hybrid states, but predicted considerably higher masses than the bag model. For the lowest mass flux-tube hybrid baryon a mass of 1.870 ± 0.100 GeV was found. In all cases the lowest mass hybrid baryon was predicted as a $J^P = 1/2^+$ state,

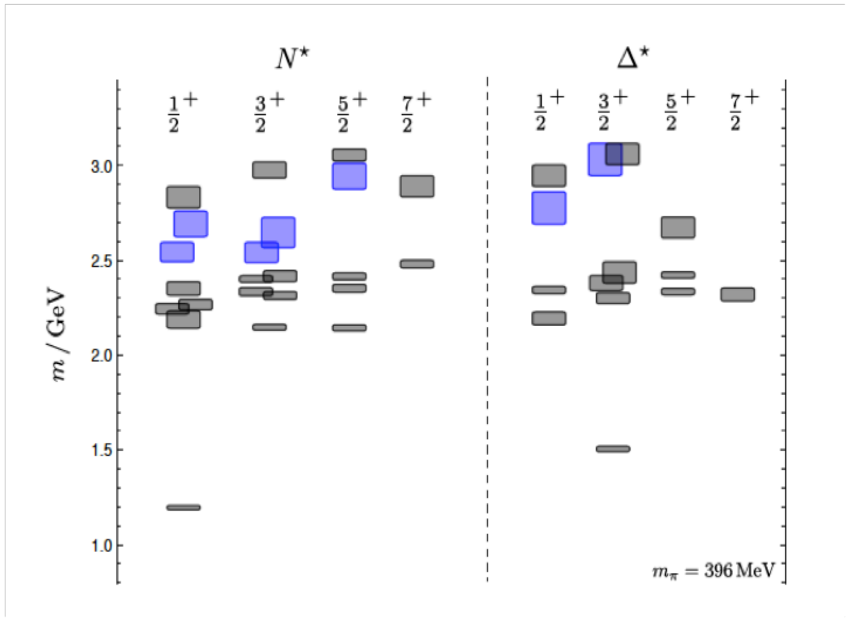

Figure 1: The light-quark baryon spectrum predicted in Lattice QCD at a pion mass of 396 MeV. The blue shaded boxes indicate states with dominant gluonic contributions. Note that both the mass of the nucleon ground state and of the $\Delta(1232)$ are shifted by nearly 300 MeV to higher masses.

i.e. a nucleon-like or Roper-like state. Hybrid baryons were also discussed in the Large N_c approximation of QCD for heavy quarks [16], which also led to the justification of the constituent glue picture used in the models. The high energy behavior of hybrid baryons was discussed in [17]. However, in contrast to hybrid meson production, which has received great attention both in theory and in experiments, the perceived difficulties of isolating hybrid baryon states from ordinary quark states led this part of the field to remain dormant for a decade.

2.2 Lattice QCD predictions

The first quenched calculations on the lattice came in 2003 [18], when the lowest gluonic 3-quark hybrid system was projected at a mass of 1 GeV above the nucleon mass, placing the lowest hybrid baryon at a mass around 2 GeV. The first LQCD calculation of the full light-quark baryon spectrum with unquenched quarks occurred in 2012 that included the projections of the hybrid nucleon N_G states and hybrid Δ_G states [7]. Figure 1 shows the projected light quark baryon spectrum in the lower mass range.

At the pion mass of 396 MeV used in this projection, the prediction for the nucleon mass is shifted by nearly 300 MeV to higher masses. In the following we take this shift into account by subtracting 300 MeV from the masses of the excited states in Fig. 1. As stated in [7], the lowest hybrid baryons, shown in Fig. 1 in blue, were identified as states with leading gluonic contributions. If hybrid baryons are not too wide, we might expect the lowest hybrid baryon to occur at masses of about 1.3 GeV above the ground state, i.e. in a mass range of 2.2 -

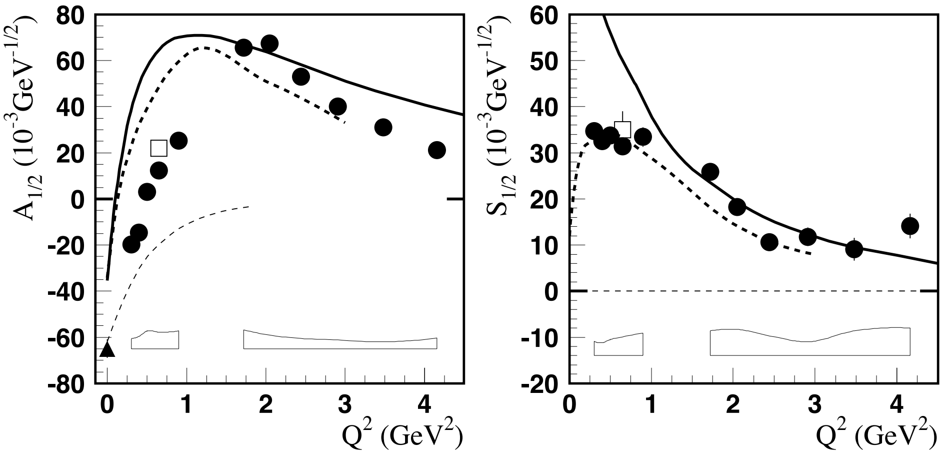

Figure 2: Electrocoupling amplitudes of the Roper resonance $N(1440)\frac{1}{2}^+$. The thin dashed lines are the constituent quark-glue model predictions for the gluonic Roper

.

2.3 GeV, a few hundred MeV above the band of radially excited $J^P = \frac{1}{2}^+$ 3-quark nucleon excitations of isospin 1/2 and thus possibly well separated from other states.

In this computation the lowest $J^P = \frac{3}{2}^+$ gluonic states are nearly mass degenerate with the corresponding $J^P = \frac{1}{2}^+$ gluonic states generating a glue-rich mass range of hybrid nucleons. If these projections hold up with LQCD calculations using near physical pion masses, one should expect a band of the lowest mass hybrid baryon states with spin-parity $\frac{1}{2}^+$ and $\frac{3}{2}^+$ to populate a relatively narrow mass band of $2.2 - 2.5$ GeV. Note, that these states fall into a mass range where no 3-quark nucleon excitations are predicted to exist from these calculations. The corresponding negative parity hybrid states, which are expected to occur at much higher masses, are not included in this graph, and are not further considered here; although they may be subject of analysis, should they appear within the kinematic range covered by this Proposal.

2.3 Hadronic couplings

Very little is known about possible hadronic couplings of hybrid baryons. One might expect an important role for final states with significant gluonic admixture, e.g. $B_G \to N\eta'$ [19], or final states containing $s\bar{s}$ contributions due to the coupling $G \to s\bar{s}$, e.g. $B_G \to K^+\Lambda$, $B_G \to N^*(1535)\pi \to N\eta\pi$, $B_G \to N\pi\pi$, $B_G \to \phi(1020)N$, and $B_G \to K^*\Lambda$. Quark-model estimates of the hadronic couplings would be helpful in selecting the most promising final state for the experimental evaluation. As long as such estimates are not available we will use a range of assumptions on the hadronic couplings to estimate the sensitivity required for definitive measurements. Assuming hadronic couplings of a few percent in the less complex final states, e.g. $K^+\Lambda$, $K^*\Lambda$, or $N\pi\pi$, we should be able to identify these states and proceed to experimentally establish their electromagnetic couplings and Q^2 dependences.

2.4 Electromagnetic couplings

Electromagnetic couplings have been studied within a non-relativistic constituent quark-gluon model, but only for two possible hybrid states, the Roper $N_G(1440)\frac{1}{2}^+$ and the $\Delta_G(1600)\frac{3}{2}^+$. In reference [20] the photoexcitation of the hybrid Roper resonance $N(1440)\frac{1}{2}^+$ was studied, and in reference [21] the electroproduction transition form factors of a hybrid Roper state were evaluated. The latter was essential in eliminating the Roper resonance as a candidate for a hybrid state, both due to the transverse helicity amplitude and its Q^2 dependence and the prediction of $S_{1/2}(Q^2) = 0$ at all Q^2. It also showed that a hybrid Roper transition amplitude $A_{1/2}$ should behave like the $A_{1/2}$ of the ordinary $\Delta(1232)$. Clearly the $S_{1/2}$ behaves differently and the $A_{3/2}$ does not exist for the Roper. Recent measurements of the electrocoupling transition amplitudes are shown in Fig. 6. Both amplitudes exhibit a Q^2 dependence that is distinctively different from the hybrid baryon prediction. Especially the scalar amplitude $S_{1/2}(Q^2)$ was found to be large while it is predicted to be suppressed in leading order for the lowest mass $\frac{1}{2}^+$ hybrid state.

The aforementioned predictions should apply to each lowest mass hybrid state with $J^P = \frac{1}{2}^+$ and $\frac{3}{2}^+$. One may ask about the model-dependence of this prediction. The transverse amplitude has model sensitivity in its Q^2 dependence and it depends on model ingredients, however, there are no ordinary 3-quark model predictions that would come even close to the predictions of the hybrid quark-gluon model. The radial excitation of the Roper resonance gives a qualitatively different prediction for $A_{1/2}(Q^2)$ compared to the hybrid excitation, where the 3-quark component remains in the ground state with only a spin-flip occurring (just as for the $N-\Delta(1232)$ transition). The suppression of the longitudinal coupling is a property of the γqG vertex and is largely independent of specific model assumptions.

The other state, $\Delta(1600)\frac{3}{2}^+$, was considered as a candidate for the lowest mass gluonic Δ_G. A result similar to the one for the hybrid Roper is found in [21] for a hybrid $\Delta_G(1600)\frac{3}{2}^+$, i.e. a fast falling $A_{1/2}(Q^2)$ and $S_{1/2}(Q^2) \approx 0$. The amplitudes at the photon point are not inconsistent with the ordinary 3-quark model calculation but are inconsistent with the hybrid baryon hypothesis. On the other hand this result is also in line with the expectation that the lowest mass hybrid states should have considerably higher masses than the first radially excited quark states. Note that there are currently no experimental results for the Q^2 dependence of the $A_{1/2}$ and $S_{1/2}$ amplitudes of this state.

3 Strategies for identifying Hybrid- and three-quark new baryon states

In this section we address the question if and how gluonic hybrid baryons are distinct from ordinary quark excitations. We will also elucidate the additional opportunities offered by the studies of exclusive electroproduction processes at different photon virtualities for the search of new baryon states both hybrid-baryons and regular three-quark so-called "missing" resonances.

Check for repetitions

Old version: In this section we address the question if and how gluonic hybrid baryons are distinct from ordinary quark excitations. As discussed in section 2.2 the lowest hybrid baryons should have isospin $I = \frac{1}{2}$ and $J^P = \frac{1}{2}^+$ or $J^P = \frac{3}{2}^+$, and their masses should be in the range of 2.20 to 2.50 GeV. This mass range must be verified once LQCD calculations with physical pion masses become available, as masses may shift with more realistic pion masses, likely to the lower mass range. Four states with $I = \frac{1}{2}$ and $J^P = \frac{1}{2}$ are predicted with dominant quark contributions and with masses below the mass of the lowest LQCD hybrid states. Of these four states two are the well known $N(1440)\frac{1}{2}^+$ and $N(1710)\frac{1}{2}^+$, and two are the less well established $N(1880)\frac{1}{2}^+$ and $N(2100)\frac{1}{2}^+$ with 2* and 1* ratings, respectively. Another state $N(2300)$ has a 2* rating, and falls right into the lowest hybrid mass band projected by LQCD. This state, if confirmed, could be a candidate for the predicted lowest LQCD hybrid state.

In order to address this question, it is necessary to confirm (or refute) the existence of the 2* state $N(1880)$ and of the 1* state $N(2100)$, and to measure the electromagnetic couplings of $N(2300)$ and their Q^2 dependence. Improved information on the lower mass states should become available in the next one or two years when the new high-statistics single- and double-polarization data from CLAS have been included into the multi-channel analysis frameworks such as the Bonn-Gatchina or Jülich/GWU approaches. Should these two states be confirmed, then any new nucleon state with $J^P = \frac{1}{2}^+$, which happens to be in the right mass range, could be a candidate for the lowest mass hybrid baryon. The $N(2300)\frac{1}{2}^+$ state has been seen at BES III only in the invariant mass $M(p\pi^\circ)$ of $\Psi(2S) \rightarrow p\bar{p}\pi^\circ$ events. In this case the production of $N(2300)$ occurs at very short distances as it emerges from heavy quark flavor $c\bar{c}$ decay. Hence the state may even be observable in single pion electroproduction $ep \rightarrow e'\pi^+ n$ and $ep \rightarrow e'p'\pi^\circ$, if it couples to photons with sufficient strength to be measurable.

In the $J^P = \frac{3}{2}^+$ sector the situation is more involved. There are two hybrid states predicted in the mass range 2.2 to 2.4 GeV, with masses above five quark model states at same J^P. Of the five states, two are well known 4* and 3* states, the $N(1720)\frac{3}{2}^+$ and the $N(1900)\frac{3}{2}^+$, respectively, and one state, the $N(2040)\frac{3}{2}^+$, has a 1* rating. Here we will have to confirm (or refute) the 1* star state and find two or three (if $N(2040)$ does not exist) more quark model state with the same quantum numbers in the mass range 1.7 to 2.1 GeV. There is one candidate $\frac{3}{2}^+$ state with mass near 1.72 GeV seen in $p\pi^+\pi^-$ electroproduction [50], whose status we will be able to pin down with the expected very high statistics data.

Possible signatures of the lowest mass hybrid baryons are:

- Resonance masses in the range 2.0 GeV $\leq W \leq$ 2.5 GeV with $I = 1/2$, and $J^P = \frac{1}{2}^+$ or $J^P = \frac{3}{2}^+$
- Q^2 dependence of the transverse helicity amplitude $A_{1/2}(Q^2)$ similar to the $\Delta(1232)\frac{3}{2}^+$ but dissimilar to radially excited states of same J^P, and
- a strongly suppressed helicity amplitude $S_{1/2}(Q^2) \approx 0$ in comparison to other ordinary 3-quark states or meson-baryon excitations.

This list of expected resonance properties may provide some initial guidance when examining new baryon states for signatures of large gluonic components, they are however not sufficient to firmly establish the hybrid nature of a state. To achieve this goal, improved modeling of other degrees-of-freedom such as meson-baryon contributions and direct calculations of electrocouplings from LQCD will be needed. The expected high statistics data

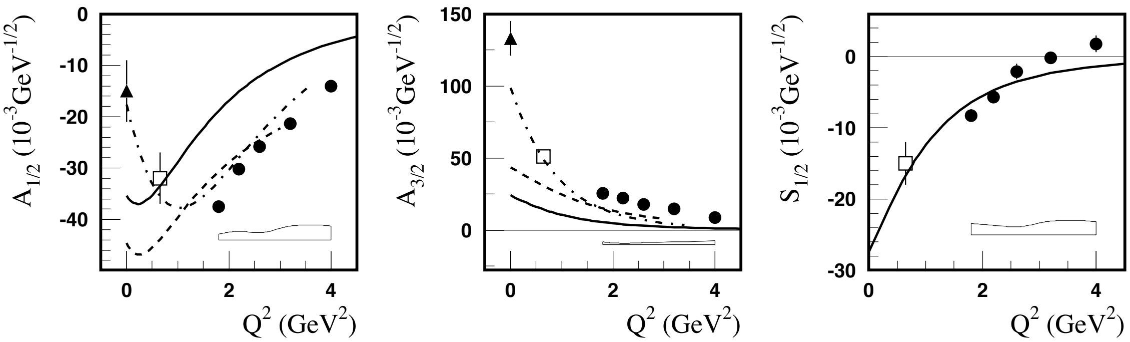

Figure 3: Electrocoupling amplitudes of the $N(1680)\frac{5}{2}^+$ resonance.

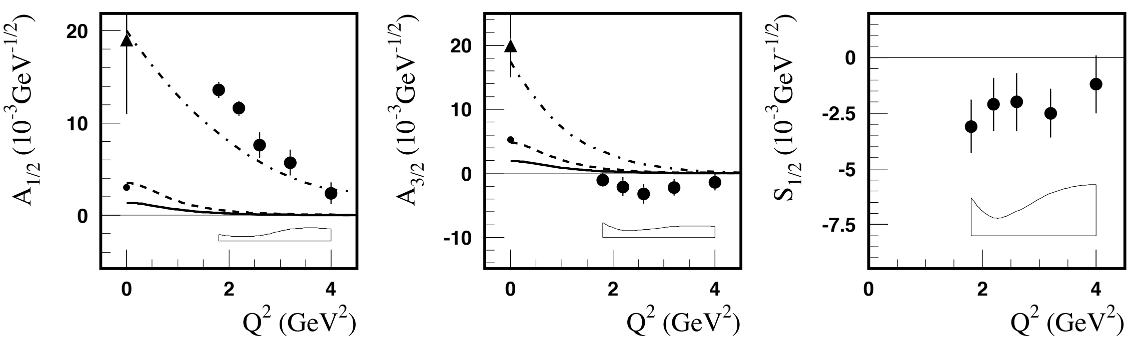

Figure 4: Electrocoupling amplitudes of the $N(1675)\frac{5}{2}^-$ resonance. Quark models predict the transverse amplitudes to be suppressed. The significant deviation of the $A_{1/2}$ amplitudes is consistent with meson-baryon contributions to the excitation strength (dashed-dotted lines).

will be used to identify any new or poorly known state, whether or not it is a candidate for a hybrid baryon state. This will aid in the identification of the effective degrees of freedom underlying the resonance excitation of all states that couple to virtual photons. old: check for repetitions

Besides the search for hybrid baryon states, there are many open issues in our knowledge of the structure of ordinary baryon excitations, that can be addressed with data taken in parallel from the same experiment. As an example we show in Fig. 3 the electrocouplings of the $N(1680)\frac{5}{2}^+$ resonance, the strongest state in the third nucleon resonance region. With the exception of the real photon point, the data are quite sparse for $Q^2 \leq 1.8$ GeV^2 and the high statistics data expected from this project would remedy the lack of experimental information and address similar situations for other states as well. Note that the very high Q^2 part will be covered by the approved JLab experiment E12-09-003.

An even more compelling example is the $N(1675)\frac{5}{2}^-$ state, where data at $Q^2 > 1.8$ GeV^2 have been published recently by the CLAS Collaboration [59]. Figure 4 shows the measured helicity amplitudes. Low Q^2 data are very important here, as for this state the quark transitions are strongly suppressed by the Moorhouse selection rule, and therefore, any non-zero value of the electrocoupling amplitudes will directly measure the strength of the meson-baryon contributions. The main data needed are single pion production $ep \to e'\pi^+n$ and $ep \to e'\pi^0p$. These processes can be accumulated with sufficiently high event rates, even with a pre-scale factor of 10 or more on the FT, should the overall event rate be too high in this 2-prong topology. As discussed in section 2.2, according to the LQCD evaluation [7] of the baryon spectrum from the QCD Lagrangian, the lowest hybrid baryons should have isospin $I = \frac{1}{2}$ and $J^P = \frac{1}{2}^+$ or $J^P = \frac{3}{2}^+$ (see Fig. 1). A difference between mass of the ground nucleon and LQCD expectation is ≈ 0.3 GeV for the computation with pion mass 0.396 GeV. However, a difference between physical mass of $N(1440)\frac{1}{2}^+$ resonance and the LQCD expectation [7] is ≈ 0.7 GeV suggesting that physics mass of the excited state can be push down by even more than 0.3 GeV, when the pion mass from LQCD is approaching the physics value. So, the masses of the lightest hybrids mass range should be in the range of 2.10 to 2.50 GeV This mass range must be verified once LQCD calculations with physical pion masses become available. Three states with $I = \frac{1}{2}$ and $J^P = \frac{1}{2}$ are predicted with dominant quark contributions and with masses below the mass of the lowest LQCD hybrid states. Of these three states two are the well known $N(1440)\frac{1}{2}^+$ and $N(1710)\frac{1}{2}^+$, and less well established $N(1880)\frac{1}{2}^+$ with 2* rating. Other states $N(2100)\frac{1}{2}^+$ and $N(2300)$ have 1* and 2* ratings, respectively, and fall right into the lowest hybrid mass band projected by LQCD. The The states $N(2100)\frac{1}{2}^+$ and $N(2300)$, if confirmed, could be the candidates for the predicted lowest LQCD hybrid state of $J^P = \frac{1}{2}$.

In the $^P = \frac{3}{2}^+$ sector the situation is more involved. There are hybrid states predicted in the mass range 2.2 to 2.4 GeV, with masses above quark model states at same J^P. Of these states, two are well known 4* the $N(1720)\frac{3}{2}^+$ and the 3* state $N(1900)\frac{3}{2}^+$, and one state, the $N(2040)\frac{3}{2}^+$, has a 1* rating. Here we will have to confirm (or refute) the 1* star state and find (if $N(2040)$ does not exist) more quark model state(s) with the same quantum numbers in the mass range 2.1 to 2.5 GeV. Among the states of spin-parity $J^P = \frac{3}{2}^+$, there is one candidate $\frac{3}{2}^+$ state with mass near 1.72 GeV seen in $p\pi^+\pi^-$ electroproduction [50], whose status we will be able to pin down with the expected very high statistics data.

In the computation [7] the lowest $J^P = \frac{3}{2}^+$ gluonic states are nearly mass degenerate with the corresponding $J^P = \frac{1}{2}^+$ gluonic states generating a glue-rich mass range of hybrid nucleons. If these projections hold up with LQCD calculations using near physical pion masses, one should expect a band of the lowest mass hybrid baryon states with spin-parity $\frac{1}{2}^+$ and $\frac{3}{2}^+$ to populate a relatively narrow mass band of $2.1 - 2.5$ GeV. Note, that these states fall into a mass range where no 3-quark nucleon excitations are predicted to exist from these calculations. The corresponding negative parity hybrid states, which are expected to occur at much higher masses, are not included in the Fig. 1, and are not further considered here; although they may be subject of analysis, should they appear within the kinematic range covered by this Proposal.

Therefore, we propose to search for the extra states of spin-parity $J^P = \frac{1}{2}^+$, $J^P = \frac{3}{2}^+$, $I = \frac{1}{2}^+$, isospin in the excited nucleon spectrum in the mass range from 2.1 GeV to 2.5 GeV. In order to conclude on their hybrid nature further studies of their hadronic decays and electrocouplings are needed, since expected spin-parities and isospin of the lowest hybrid states are the same as for three-quark "missing" resonances.

Expected hadronic decays of hybrid baryons were discussed in the Section 2.3. Because of the coupling of the glue admixture to the $q\bar{q}$ pair, the hybrid baryons will manifest in the channels with strange mesons and baryons, as well as in the electroproduction of multi-meson final states with more than single mesons. We included into our Proposal those of

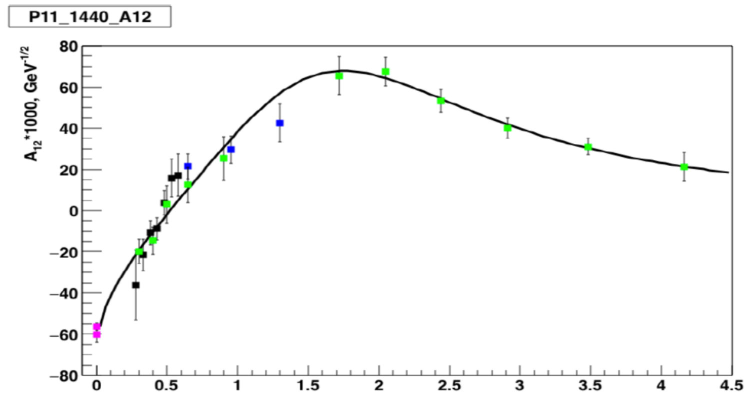

Figure 5: Interpolation of the $N(1440)1/2^+$ electrocouplings from the CLAS data on $N\pi$ (green circles) [6] and $\pi^+\pi^-p$ [26, 51] (black and blue squares) exclusive electroproduction off protons. The results at the photon point are taken from [1, 27]

the aforementioned channels which we already studied in details previously and included into the future N^* studies with the CLAS12 [2, 3], i.e. $K^+\Lambda$, $K^+\Sigma$ and $\pi^+\pi^-p$. Later on these studies may be extended by the exploration of other electroproduction channels such as $\phi(1020)N$, $K^*\Lambda$.

Studies of excited nucleon state electrocouplings in a wide range of photon virtualities is proven to be the effective tools in establishing the active degrees of freedom contributing to the N* structure at different distances [2, 3, 24–26]. The information on the $\gamma_v NN^*$ electrocoupling evolution with Q^2 becomes critical in the search for hybrid baryons. The distinctively different Q^2-evolution of the hybrid-baryon electrocouplings is expected considering the different color-multiplet assignments for the quark-core in a regular versus a hybrid baryon, i.e. a color singlet and octet, respectively.

The electroproduction transition form factors of a Roper state assuming the presence of glue (hybrid Roper) were evaluated in [21]. This studies demonstrated that for hybrid Roper longitudinal electrocouplings should be much smaller than transverse $A_{1/2}$ electrocouplings. Virtually $S_{1/2}$ electrocouplings should be comparable with zero at the scale of the transverse electrocouplings. It also showed that a hybrid Roper transition amplitude $A_{1/2}$ should behave like the $A_{1/2}$ of the ordinary $\Delta(1232)$. The aforementioned predictions should apply to each lowest mass hybrid state with $J^P = \frac{1}{2}^+$ and $J^P = \frac{3}{2}^+$. The suppression of the longitudinal coupling is a property of the γqG vertex and is largely independent of specific, which is purside of the current model assumptions.

Based on quark counting rules [**?**], we expect that electrocouplings of hybrid baryons should decrease with photon virtuality Q^2 more rapidly than for the regular three-quark nucleon resonance because of the extra- constituent. So, the low photon virtualities offer a preferential regime for the studies of hybrid-baryons. In our Proposal we are planning to explore the range of $Q^2 < 2.0$ GeV^2 with particular focus for hybrid baryon search at $Q^2 <$

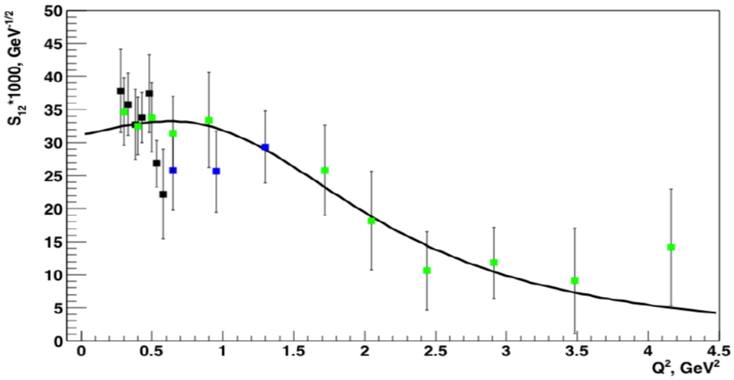

Figure 6: Interpolation of the $N(1710)1/2^+$ electrocouplings from the CLAS data on $N\pi$ (green circles) [28] exclusive electroproduction off protons. The results at the photon point are taken from [1, 27]

1.0 GeV^2.

In a case of $J^P = \frac{3}{2}^+$ all three electrocouplings $A_{1/2}$, $S_{1/2}$ and $A_{3/2}$ contribute to the state electroexcitations. The prediction on the relations between $A_{1/2}$, $A_{3/2}$, and $S_{1/2}$ hybrid electrocouplings exist only for the area large photon virtuality [17] which is outside of the current study scope. In the future the $A_{1/2}$, $S_{1/2}$ and $A_{3/2}$ hybrid electrocouplings will be evaluated within.... at $Q^2 < 2.0$ GeV^2 as a part of the commitment of....

In order to identify hybrid-baryon we are looking for its electrocouplings behavior which should have distinctively different features in comparison with already established from the CLAS results [3] electrocouplings of three-quark resonances of $J^P = \frac{1}{2}^+$ shown in Fig 6 and of $J^P = \frac{3}{2}^+$ shown in Fig 8

3.1 Signature of the hybrid-baryon in the experimental data

We propose to search for the new baryon states in the exclusive $K^+\Lambda$ and $K^+\Sigma$ and $p\pi^+\pi^-$ electroproduction at the photon virtualities from 0.05 GeV^2 to 1.0 GeV^2. Possible signatures of the lowest mass hybrid baryons are:

- Almost degenerated pairs of the states with isospin $I = 1/2$, and spin-parities $J^P = \frac{1}{2}^+$ or $J^P = \frac{3}{2}^+$ and the masses in the range 2.0 GeV $\leq W \leq$ 2.5 GeV. The hybrid-states of both spin-parities should belong to the two spin-parity bands with well established lowest $N(1440)1/2^+$ and $N(1720)3/2^+$ resonances and with the regular three-quark resonances of masses above and below the hybrid-baryon mass.

- particular features in Q^2 dependence of hybrid electrocouplings related to the color octet assignment for three constituent quarks including: dominance of the transverse over longitudinal amplitudes, similarity of the transverse helicity amplitudes $A_{1/2}(Q^2)$

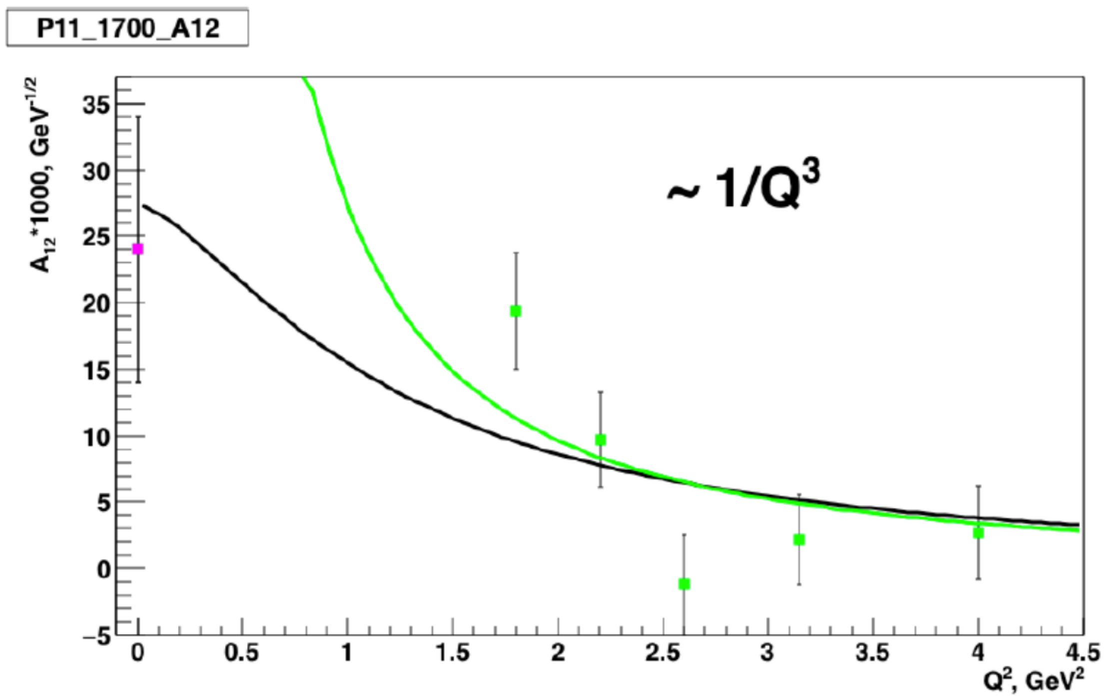

Figure 7: Interpolation of the $N(1720)3/2^+$ electrocouplings from the CLAS data on $\pi^+\pi^-p$ [29] exclusive electroproduction off protons [46]. The results at the photon point are taken from [27, 29]

for the hybrid-baryon and for the $\Delta(1232)\frac{3}{2}^+$ but dissimilar to the three-quark excited states of same J^P, and

- a strongly suppressed helicity amplitude $S_{1/2}(Q^2) \approx 0$ in comparison to other ordinary 3-quark states.

3.2 Search for the three-quark new baryon states

Advanced studies of the data on exclusive meson photoproduction off protons carried out within the framework of the global multi-channel amplitude analysis developed by the Bonn-Gatchina group [30–32] revealed the signals from many new baryon states in the mass range from 1.7 GeV to 2.5 GeV. These states were included to the PDG [1] with the status from one to three star states. Notably, the most prominent signals from new states come from analyses of the CLAS [33–36], ELSA [37], MAMI [38] and GRAAL [40?] data on KY electroproduction. Studies of KY as well as $\pi^+\pi^-p$ exclusive electroproduction channels extend considerably our capability in establishing of the excited nucleon state spectrum, including both regular three-quark and exotic hybrid states.

The new baryon states, if they are excited in s-channel should be seen in exclusive reactions both with the real and virtual photons in the same final states. Furthermore, their masses, total decay widths, partial decay widths to different final states should be Q^2-

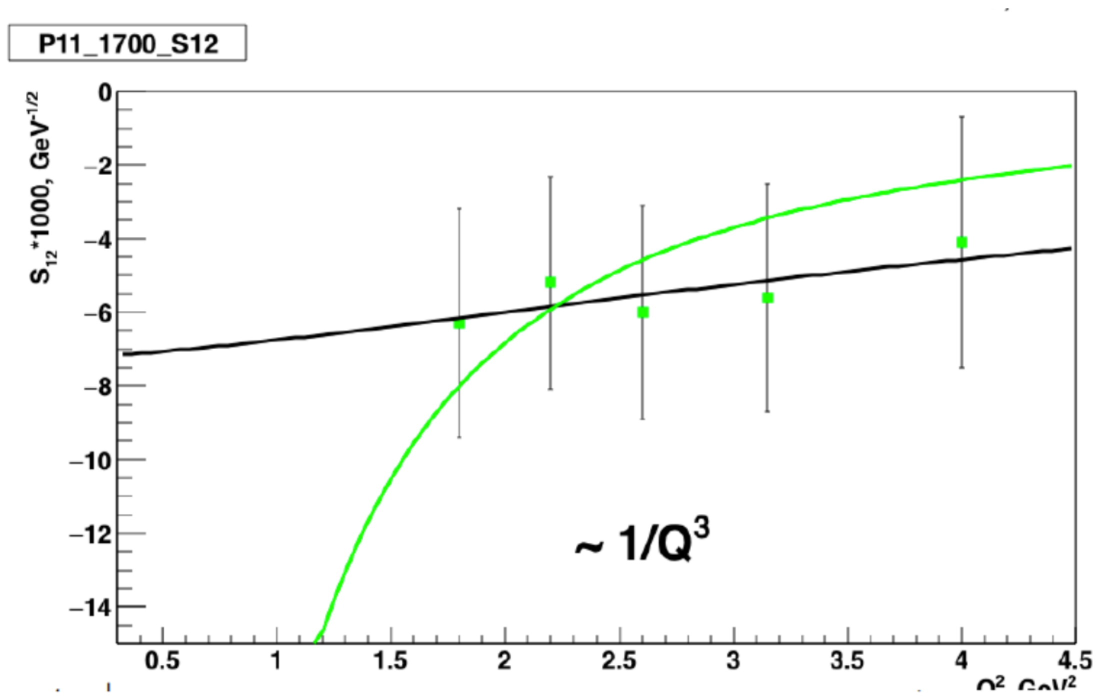

Figure 8: Interpolation of the $N'(1720)3/2^+$ electrocouplings from the CLAS data on $\pi^+\pi^-p$ [29] exclusive electroproduction off protons [46]. The results at the photon point are taken from [27, 29]

independent. The values of $\gamma_v pN^*$ electrocouplings obtained independently from analyses of different exclusive channels with completely different non-resonant contributions should be the same. Consistent results on resonance masses, $\gamma_v pN^*$ electrocouplings for all exclusive decay channels under study, and Q^2-independent partial hadronic decay widths, over the full covered Q^2-range, will offer convincing evidence for the existence of new states. These studies offer model independent way to prove not only the existence of new excited nucleon states but also their nature as the s-channel resonances eliminating the alternative interpretations for the structures observed in the kinematics dependencies of the observables as complex coupled channel effects, dynamical singularities for the non-resonant amplitudes, kinematic reflections, etc.

This strategy was successfully employed in the recent analysis of the $\pi^+ pi^- p$ preliminary photo- and electroproduction cross sections [50] from the CLAS carried out combined within the framework of meson-baryon reaction model JM [29]. It was found that in order to describe both photo- and electroproduction data at W around 1.7 GeV keeping $\pi\Delta$ and ρp hadronic decay widths of all contributing resonances Q^2-independent, new baryon state $N'(1720)3/2^+$ state is needed with almost the same mass , total widths and the same spin-parity as for the conventional $N(1720)3/2^+$ resonances, but with completely different branching fractions for the hadronic decay to the $\pi\Delta$ and ρp final state and Q^2-evolution of its $\gamma_v pN^*$ electrocouplings.

The studies of exclusive KY, $\pi^+\pi^-p$ electroproduction channels at $Q^2 < 2.0$ GeV^2 with maximal virtual photon flux ever achieved in exclusive electroproduction will allow us to solidify the results on the spectrum of excited nucleon states, confirming or ruling out the signal of "missing" resonances observed in exclusive photoproduction. Furthermore, for the first time the information on $\gamma_v pN^*$ electrocouplings of new baryon states will become available offering an access to the structure of "missing" resonances elucidating their differences from the conventional resonances. Finally we want to note that the studies of two major exclusive $N\pi$ and $\pi^+\pi^-p$ electroproduction channels with CLAS revealed the relative growth of the resonant contributions with Q^2 in both channel. So, use of the high intensity virtual photon flux of the proposed experiment may be even preferential for new baryon state search in comparison with the photoproduction. It still remain to be seen which range of photon virtualities is the most suitable for the discovery of new excited nucleon states.

3.3 Amplitude analyses of measured observables in a search for new baryon states.

In the analyses of the future experimental data we will apply the amplitude analyses methods for the resonance search and extraction of the resonance parameters. We will employ the global fit of all exclusive channels studied with the CLAS12 in the kinematics of out interest with a focus on new baryon state search within the framework of coupled channel approaches. We also planning to extract of the resonance parameters from the independent analyses of KY, $\pi^+\pi^-p$ exclusive electroproduction off protons carried our within the framework of the reaction models for description of these exclusive channels. Consistent results on the resonant parameters determined from independent analyses of different exclusive meson electroproduction channels and extracted from the global multi-channel fit of all available data will offer strong and almost the model independent evidences for the new state existence and reliable extraction of their parameters. Note, that in order to apply the coupled channel approaches to the analyses of KY, $\pi^+\pi^-p$ exclusive electroproduction data, the information on $N\pi$ electroproduction off protons is also needed. The $N\pi$ exclusive channels dominate at $W < 1.6$ GeV and remain have much bigger cross sections in comparison with the KY electroproduction in the entire kinematics area of our interest. The events from $N\pi$ exclusive channels will be collected simultaneously with the measurement of KY, $\pi^+\pi^-p$ exclusive electroproduction off protons offering the information on the $N\pi$ channel observables.

Advanced amplitude analysis approach for extraction of the nucleon resonance parameters from the global analysis of the photoproduction data, which include almost all relevant in resonance excitation region exclusive meson photoproduction channels off nucleons, has been developed by Bonn-Gatchina group [30–32]. In this approach production amplitudes are decomposed over the set of partial waves. The partial wave amplitudes are parameterized fully accounting for the restrictions imposed by the general unitarity and analyticity conditions, employing K- and D-matrix approaches for the final state interactions while for the photoproduction amplitudes the P-vector approach is used. In a case of pronounced t-channel contributions, Reggeized t-exchanges are incorporated to the photoproduction amplitudes. The hadronic final state interaction are treated employing phenomenological parameterisation, for the respective amplitudes. The resonance parameters were determined from the global

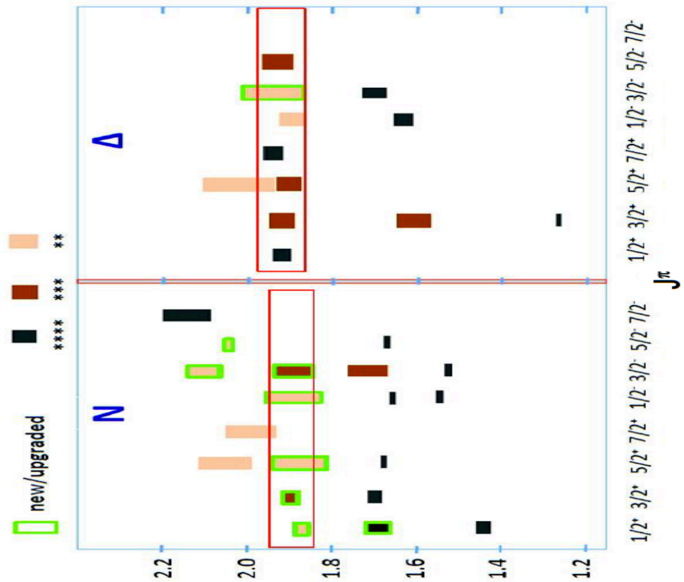

Figure 9: Recent results on the spectrum of excited nucleon states [1]. Signals from the states shown in green boxes were observed in global multi-channel analysis of exclusive meson electroproduction data carried out within the framework of Bonn-Gatchina approach[30–32].

fit of all available exclusive photoproduction data augmented by the fit of hadroproduction channels for the final states under studies. Application of the Bonn-Gatchina approach to the global analysis of the dominant part of exclusive meson photoproduction data measured with the CLAS and worldwide provided information on masses, widths, photocouplings and hadronic decay parameters for most excited nucleon states in the mass range up to 3.0 GeV. This analyses revealed the signal from around ten new baryon states, reported in the PDG [1] with the status from one- to three- stars and shown in Fig. 9.

Extension of this approach for description of exclusive electroproduction including KY channels represent the part of the commitment of the Bonn-Gatchina group reported in [41]. Bonn-Gatchina approach extended for analysis of the exclusive electroproduction will be used for extraction of resonance parameters and search for new baryon states in the proposed experiment. The aforementioned extension will be vital in order to check the signals from new baryon states observed in the exclusive meson photoproduction and shown in Fig. 9 independently in the exclusive electroproduction processes confirming or rejecting the candidate-states observed in the photoproduction. It is a critical part of effort in finalizing the long-term program on exploration of the spectrum of excited nucleon states and simultaneously the new avenue extending our knowledge on variety of hadrons in the Nature through the search for hybrid-baryons.

An advanced dynamical coupled-channel model (DCC) has been developed by the Argonne-Osaka collaboration for combined analysis of the world data for $\pi N, \gamma N \rightarrow \pi N, \eta N, K\Lambda, K\Sigma$ $N\pi\pi$ photo-electro and hadroproduction with a goal of extracting resonance parameters [42, 43]. The DCC approach incorporates three level diagrams derived from effective Lagrangian for the resonant and non-resonant contributions in the photo-/electroproduction as well as in the final state hadronic interactions. The amplitudes for all exclusive channels are fully consistent with the restrictions imposed by the general unitarity and analyticity conditions. This is the only coupled channel approach capable of describing the $N\pi\pi$ photo-/electro-/hadro- production in accord with a general unitarity condition. In order to fulfill the unitarity restrictions, the meson-baryon interactions from the non-resonant amplitudes of all included exclusive processes, the so-called meson-baryon cloud, are incorporated to the electromagnetic and hadronic vertices of nucleon resonances together with direct resonance decays to the $\gamma_{r,v}p$ and meson-baryon final states (bare verticies). Analysis of the observables within the framework of the DCC approach allows us not only to extract the full dressed resonance electromagnetic and hadronic decay amplitudes, but also to disentangle between the contributions from the meson-baryon cloud and bare vertices associated to the quark core part in the nucleon resonance structure. The DCC approach is capable of providing valuable insight to the structure of excited nucleon states. The DCC-model currently is the only available worldwide coupled channel approach that provides the results on $N \to \Delta(1232)3/2^+$ transition form factors at Q^2 up to 7. GeV^2 [3] and $N(1440)1/2^+$ electrocouplings at Q^2 up to 3 GeV^2 [44]. Argonne-Osaka DCC-model will be employed in analyses of the data of the proposed experiment with a goal to observe manifestation of new excited nucleon state and to extract $\gamma_v pN^*$ electrocouplings of the established and new baryon states. This model will allow us to fully account in extraction of $\gamma_v pN^*$ electrocouplings from KY channels for the impact of the final state interaction with the open channels for which the electroproduction cross sections are much larger, i.e. $N\pi$, and $N\pi\pi$. Furthermore, it is the only available worldwide approach capable to account for the complexity of the final state interactions in the $\pi^+\pi^-p$ final state in a way consistent with the unitarity.

So far, most of the results on $\gamma_v pN^*$ electrocouplings have been extracted from independent analyses of π^+n, π^0p, and $\pi^+\pi^-p$ exclusive electroproduction data off the protons.

The $N\pi$ data have been analyzed within the framework of two conceptually different approaches: a unitary isobar model (UIM) and dispersion relations (DR) [6, 28]. The UIM describes the $N\pi$ electroproduction amplitudes as a superposition of N^* electroexcitations in the s-channel, non-resonant Born terms and ρ- and ω- t-channel contributions. The latter are reggeized, which allows for a better description of the data in the second- and third-resonance regions. The final-state interactions are treated as πN rescattering in the K-matrix approximation [**?**]. In the DR approach, dispersion relations relate the real to the imaginary parts of the invariant amplitudes that describe the $N\pi$ electroproduction. Both approaches provide good and consistent description of the $N\pi$ data in the range of $W < 1.7$ GeV and $Q^2 < 5.0$ GeV^2, resulting in $\chi^2/\text{d.p.} < 2.9$. In the proposed this approach will be used for evaluation of the $N\pi$ electroproduction amplitudes needed as the input for the aforementioned global multi-channel analyses of the KY and $\pi^+\pi^-p$ exclusive electroproduction data.

The $\pi^+\pi^-p$ electroproduction data from CLAS [46, 52] provide for the first time information on nine independent single-differential and fully-integrated cross sections binned in W and Q^2 in the mass range $W < 2.0$ GeV and at photon virtualities of 0.25 GeV$^2 < Q^2 <$ 1.5 GeV^2. The analysis of the data allowed us to develop the JM reaction model [8, 26, 51] with the goal of extracting resonance electrocouplings as well as $\pi\Delta$ and ρp hadronic decay widths. This model incorporates all relevant reaction mechanisms in the $\pi^+\pi^-p$ final-state channel that contribute significantly to the measured electroproduction cross sections off protons in the resonance region, including the $\pi^-\Delta^{++}$, $\pi^+\Delta^0$, $\rho^0 p$, $\pi^+N(1520)\frac{3}{2}^-$, $\pi^+N(1685)\frac{5}{2}^+$, and $\pi^-\Delta(1620)\frac{3}{2}^+$ meson-baryon channels as well as the direct production of the $\pi^+\pi^-p$ final state without formation of intermediate unstable hadrons. In collaboration with the JPAC [?] the special approach has been developed allowing us to remove the contributions from the s-channel resonances to the reggeized t-channel non-resonant terms in $\pi^-\Delta^{++}$, $\pi^+\Delta^0$, $\rho^0 p$ electroproduction amplitudes. The contributions from well established N* states in the mass range up to 2.0 GeV were included into the amplitudes of $\pi\Delta$ and ρp meson-baryon channels by employing a unitarized version of the Breit-Wigner ansatz [51]. The JM model provides a good description of $\pi^+\pi^-p$ differential cross sections at $W < 1.8$ GeV and 0.2 GeV$^2 < Q^2 < 1.5$ GeV^2 with χ^2/d.p. < 3.0. The achieved quality of the CLAS data description suggest the unambiguous and credible separation between the resonant/non-resonant contributions achieved fitting the CLAS data [26]. The credible isolation of the resonant contributions makes it possible to determine the resonance electrocouplings and $\pi\Delta$, and ρN decay widths from the resonant contributions employing for their description the amplitudes of the unitarized Breit-Wigner ansatz [51] that fully accounts for the unitarity restrictions on the resonant amplitudes. This model will be used in the proposed experiment for analyses of exclusive $\pi^+\pi^-p$ electroproduction allowing us to determine electrocouplings of most excited nucleon since almost all nucleon resonances have substantial hadronic decays to the $N\pi\pi$ final states. Capability of the JM model to pin down new baryon states was demonstrated in the combined studies of exclusive $\pi^+\pi^-p$ photo- and electroproduction [29] which provided convincing evidence for new baryon state $N(1720)3/2^+$

The model for description of the KY exclusive photo- and electroproduction channels "regge-plus-resonance" (RPR) has been developed by the Ghent group [9, 57]. In this model full production amplitude is described by the superposition of eight resonances and the non-resonant contribution. The non-resonant amplitudes represent the sum of t-channel exchanges by K- and K^*-Regge trajectories. The model provided a good description of KY photoproduction data. It reproduces the gross features in Q^2-evolution for the exclusive unpolarized structure functions. We are planning to use this model for extraction of the resonance electrocouplings from exclusive KY electroproduction data after the model upgrade allowing improved description of the structure functions. The development in this direction was presented in [45].

3.4 Modeling the hybrid baryon contribution to exclusive KY and $\pi^+\pi^-p$ electroproduction off protons.

To prove the feasibility to observe hybrid baryons we have studied the effect of implementing the contribution of the two lightest hybrid states of $\approx$ 2.6 GeV mass with spin-parities $J^P = \frac{1}{2}^+$ and $\frac{3}{2}^+$ to the reaction model of both $K\Lambda$ and $K\Sigma$ electroprodution.

For mass estimations of the hybrid baryon we have considered Lattice QCD predictions that were carried out with a pion mass above the physical value; we have corrected the predicted hybrid baryon masses by employing mass shifts for both states towards smaller values, which can be expected when the physical pion mass is reached. The mass shift for the lowest hybrid baryon with $J^P = \frac{1}{2}^+$ spin-parity can be estimated by the difference between the LQCD result [7] for the mass of the lightest nucleon of spin-parity $J^P = \frac{1}{2}^+$ and the measured value of the proton mass, Δ_1=0.3 GeV. For the lowest hybrid state with

$J^P = \frac{3}{2}^+$, the mass shift can be estimated by the differences between the mass of the lightest LQCD resonance with $J^P = \frac{3}{2}^+$ and the physical mass of the $N(1720)\frac{3}{2}^+$ four star resonance, Δ_2=0.5 GeV.

Therefore, we have modeled the hybrid baryons contributions considering spin-parities $J^P = \frac{1}{2}^+$ and $J^P = \frac{3}{2}^+$ in the mass range from 2.1 to 2.3 GeV. According to the RPP14 results [1] on the resonance parameters in the mass range around 2.0 GeV, we adopted for the total decay width of hybrid baryons a range from 250 to 300 MeV and for their branching fraction (BF) to the KY and $\pi^+\pi^-p$final states the value of 5%.

The excitation of a single hybrid resonance in the helicity representation $\langle\lambda_f\,|T_r|\,\lambda_\gamma\lambda_p\rangle$ may be expressed using a relativistic Breit-Wigner (BW) ansatz:

$$M_{\lambda_\gamma}^{\lambda_p\lambda_f} = \langle\lambda_f\,|T_r|\,\lambda_\gamma\lambda_p\rangle = \frac{\langle\lambda_f\,|T_{dec}|\,\lambda_R\rangle\langle\lambda_R\,|T_{em}|\,\lambda_\gamma\lambda_p\rangle}{M_r^2 - W^2 - i\Gamma_r M_r}, \tag{1}$$

where M_r and Γ_r are the resonance mass and total width, respectively; we assumed both total and partial decay widths to be energy independent.

The matrix elements $\langle\lambda_R\,|T_{em}|\,\lambda_\gamma\lambda_p\rangle$ and $\langle\lambda_f\,|T_{dec}|\,\lambda_R\rangle$ are the electromagnetic production and hadronic decay amplitudes of the N^* with helicity $\lambda_R = \lambda_\gamma - \lambda_p$, in which λ_γ and λ_p stand for the helicities of the photon and proton in the initial state, and λ_f represents the helicity of final-state hadron in the N^* decays.

The explicit form of the $\langle\lambda_f\,|T_r|\,\lambda_\gamma\lambda_p\rangle$ amplitudes is reported in Appendix B. This contribution has been added to the most advanced reaction models of KY and $\pi^+\pi^-p$ exclusive electroproduction cross sections:

- in the case of the KY channel we considered as a reference the Regge plus resonsnce model (RPR-2011)[9, 22] in which reggeized non-resonant amplitudes and the contributions from the established N^* states have been used to describe both KY photo- and electro-production. The web-site [23] provides a full set of KY electroproduction observables off proton (Model A). The contribution of the new hybrid baryon state in the virtual-photon-proton s-channel, described by 1, has been coherently added to the PRP-2011 model at the amplitude level, and the resulting cross-section, including polarization terms, has been evaluated as a function of the hybrid resonance electrocoupling values (Model B).

- in the case of the $\pi^+\pi^-p$ channel we considered the effect of an incoherent superposition of the hypothetical cross sections due to new hybrid baryon state to the most updated version of the JM model [8, 46–48].

In both cases the resulting cross sections have been used inside an event generator to determine the minimum electro-coupling strength of the hybrid baryons that would be observable in the proposed experiment. Details are shown in the next sections.

Old version to merge and partially move to the appendix.

Comparing the CMS angle distributions of the final kaons simulated according to models A and B will allow us to determine the minimal absolute values of the hybrid baryon electroexcitation amplitudes that are needed to re-identify them in the analysis of the reconstructed data. We will focus on exploration of feasibility to observe the lightest hybrid baryons of minimal decay widths, that makes the expected signals from such hybrid states the most pronounced.

The cross sections integrated over the angle ϕ_K produced by a hybrid baryon state can be evaluated from the resonant hybrid electroexcitation amplitudes according to (27,29) in the Appendix, replacing the full two-body amplitudes by the resonant contributions from the hybrid resonance. For the particular purpose of the cross section evaluation for the event generator we employ the energy independent total/partial resonance decay widths.

Inserting the production amplitudes (??), (31), and (??) for a single resonance, which in this case is a hybrid baryon candidate, into the currents determined by (29), leads to the final expressions for the transverse $\frac{d\sigma_{T_H}}{d(-cos(\theta_K))}$ and the longitudinal $\frac{d\sigma_{L_H}}{d(-cos(\theta_K))}$ ϕ_K integrated single-differential cross section for KY electroproduction off unpolarized protons for the hybrid state electroexcitation from (27) with density matrices for the initial and the final states determined by (22) :

$$\frac{d\sigma_{T_H}}{d(-\cos(\theta_K))} = \frac{4\pi\alpha}{4K_L M_N}\frac{1}{2}\frac{1}{2}\sum_{\lambda_\gamma=\pm1,\lambda_p,\lambda_f}\frac{\langle\lambda_R\,|T_{em}|\,\lambda_\gamma\lambda_p\rangle^2\langle\lambda_f|T_{dec}^{J_r}|\lambda_R\rangle^2 d_{\mu\nu}^{J_r^2}(\cos\theta_K)}{(M_r^2-W^2)^2+(\Gamma_r M_r)^2}\frac{q_K}{2\pi 4W},$$

$$\frac{d\sigma_{L_H}}{d(-\cos(\theta_K))} = \frac{4\pi\alpha}{4K_L M_N}\frac{1}{2}\sum_{\lambda_\gamma=0,\lambda_p,\lambda_f}\frac{\langle\lambda_R\,|T_{em}|\,\lambda_\gamma\lambda_p\rangle^2\langle\lambda_f|T_{dec}^{J_r}|\lambda_R\rangle^2 d_{\mu\nu}^{J_r^2}(\cos\theta_K)}{(M_r^2-W^2)^2+(\Gamma_r M_r)^2}\frac{q_K}{2\pi 4W}, \quad (2)$$

$$\mu = \lambda\gamma - \lambda_p.$$
$$\nu = -\lambda_Y,$$

Resonance electroproduction $\langle\lambda_R\,|T_{em}|\,\lambda_\gamma\lambda_p\rangle$ and hadronic decay $\langle\lambda_f|T_{dec}^{J_r}|\lambda_R\rangle$ amplitudes are determined by (??) and (31), respectively.

Assuming only contribution from unpolarized structure functions described in the Appendix A by (23,28), the two fold differential cross sections produced by the hybrid resonance $\frac{d\sigma_H}{d\Omega_K}$ can be computed as:

$$\frac{d\sigma_H}{d\Omega_K} = \frac{1}{2\pi}[\frac{d\sigma_{T_H}}{d(-\cos(\theta_K))} + \epsilon_L\frac{d\sigma_{L_H}}{d(-\cos(\theta_K))}]. \quad (3)$$

Differential cross sections computed according to (2,3) should be added incoherently to the model [9, 22, 23] differential cross sections in order to obtain differential cross sections for KY electroproduction according to model B, which accounts for the contributions from hybrid baryon state. In both model A and model B they should be converted to the four-fold measurable electroproduction cross sections employing (16) of Appendix A. These measurable cross sections should be used in the event generator for the simulation of KY events produced in electron scattering off protons with and without hybrid baryon contributions.

The difference in the angular distributions of the reconstructed KY events simulated in the models A and B will tell us whether a given hybrid baryon state can be observed.

In order to quantify the statistical significance of the difference between the exclusive KY event distributions over the θ_K, ϕ_K CMS angles as simulated according to the models A and B, the following $\chi^2/d.p.$ definition will be used:

$$\chi^2/d.p. = \frac{1}{N_{d.p.}}\sum_{\theta_i,\phi_j,W_k}\frac{(N_{B_{i,j,k}} - N_{A_{i,j,k}})^2}{\delta_{i,j,k}^2}, \quad (4)$$

where $N_{A_{i,j,k}}$, $N_{B_{i,j,k}}$ are the numbers of KY events in the kinematic bins of θ_i, ϕ_j and W_k simulated in the models A and B, respectively, taking into account the CLAS12 acceptance,

θ_i and ϕ_i stand for the polar and azimuthal emission angles of kaon in the CMS frame, the sum runs over all bins over θ_K, ϕ_K, and W within any given bin of Q^2. The $N_{d.p.}$ is the total number of θ, ϕ, and W bins that are included in the sum (13). The values of $\chi^2/d.p.$ should be evaluated independently in each Q^2 bin. The θ_K- and ϕ_K CMS angles are running from 0^0 to 180^0 and from 0^0 to 360^0, respectively. The sum over W ranges from 1.9 GeV to 2.4 GeV, which is predicted to be the most sensitive range for low-lying hybrid baryon contributions. Assuming that the statistical uncertainties dominate, the uncertainties for the differences ($N_{B_{i,j,k}}$-$N_{A_{i,j,k}}$) between the event distributions simulated in the models B and A, respectively, can be evaluated as:

$$\delta_{i,j,k} = \sqrt{N_{A_{i,j,k}} + N_{B_{i,j,k}}}. \tag{5}$$

We will investigate hybrid baryon states with spin-parities $J^P = \frac{1}{2}^+$ and $\frac{3}{2}^+$. Electroexcitation of the former state can be described by two electrocouplings $A_{1/2}$ and $S_{1/2}$, while the latter should be described by three electrocouplings, $A_{1/2}$, $S_{1/2}$, and $A_{3/2}$. The definitions of all electrocouplings can be found in the review [2]. Information on the expected Q^2-evolution of the aforementioned electrocouplings for hybrid states is, to the best of our knowledge, currently not available. We will vary the hybrid baryon electrocouplings to determine their minimal absolute values above which the signal from the hybrid baryon can be observed in the difference between the angular distributions with and without hybrid baryon contributions. These studies will be independently done in each Q^2 bin of the proposed experiment.

The following restrictions will be imposed in the variation of the hybrid baryon electrocouplings, assuming positive values of all electrocouplings.

- **the hybrid baryon of $\frac{3}{2}^+$ spin-parity:** Three electrocouplings $A_{1/2}$, $S_{1/2}$, and $A_{3/2}$ will be computed varying the positive parameter A as:

$$\begin{aligned} A_{1/2} &= A, \\ S_{1/2} &= AQ, \\ A_{3/2} &= A/Q^2, \\ Q &= \sqrt{Q^2} \end{aligned} \tag{6}$$

  The relations (6) for the hybrid baryon electrocouplings have been used in the modeling [17] of the hybrid baryon signatures.

- **Hybrid baryon with $\frac{1}{2}^+$ spin-parity:** Electrocouplings will be varied under two assumptions: a) $S_{1/2}$=0 GeV$^{-1/2}$ as predicted by model [21] for the hybrid N(1440)1/2$^+$ resonance, and b) the relations (6) with $A_{3/2}$=0 GeV$^{-1/2}$ will be employed.

The $\chi^2/d.p.$ values, calculated according to (13) will elucidate the feasibility of hybrid baryon observation. The $\chi^2/d.p.$ values above 2 will be considered as the statistically significant signals for hybrid baryon states. Consequently, the minimal absolute values of hybrid baryon electocouplings, above which $\chi^2/d.p.$ becomes larger than 2, will be treated as the minimal values of hybrid electrocouplings, above which the signal from a hybrid baryon can be observed in the proposed experiment.

Contribution from JPAC on Regge for KY, and......

3.5 Search for the hybrid-baryon signal employing the moment expansion

. The analysis using the Legendre moments proved to be a good way to distinguish signal from background. Legendre moments are defined as:

$$P_m = \frac{2m+1}{2}\int_{-1}^{1} L_m \sigma(x)dx \tag{7}$$

where

$$\begin{aligned}
&x = cos\theta_k \\
&L_m(x) = \sum_{j=0}^{m} a_{mj}x^j \\
&a_{mj} = (-1)^{(m-j)/2}\frac{1}{2^m}\frac{(m+j)!}{(\frac{m-j}{2})!(\frac{m+j}{2})!j!} \\
&m-j = even
\end{aligned} \tag{8}$$

The first seven Legendre polynomial functions are:

$$\begin{aligned}
&L_0 = 1 \\
&L_1 = cos\theta \\
&L_2 = \frac{1}{2}(3cos\theta^2 - 1) \\
&L_3 = \frac{1}{2}(5cos\theta^3 - 3cos\theta) \\
&L_4 = \frac{1}{8}(35cos\theta^4 - 30cos\theta^2 + 3) \\
&L_5 = \frac{1}{8}(63cos\theta^5 - 70cos\theta^3 + 15cos\theta) \\
&L_6 = \frac{1}{16}(231cos\theta^6 - 315cos\theta^4 + 105cos\theta - 5)
\end{aligned} \tag{9}$$

They are related to the coefficients C_l of the cross section expansion in terms of the orthogonal Legendre polinomials:

$$\sigma(x) = \sum_i C_l(Q^2, W)L_i(cos\theta_i^*) \tag{10}$$

The highest is the order of the Legendre moments, the highest is sensitivity to the appearence of the baryonic resonances. .... to be completed

4 The Experimental program

4.1 The CLAS12 detector

The experimental program will use the CLAS12 detector, shown in Fig. 10, for the detection of the hadronic final state. CLAS12 consists of a Forward Detector (FD) and the Central

Detector (CD). The Forward Detector is comprised of six symmetrically arranged sectors defined by the six coils of the toroidal superconducting magnet. Charged particle tracking is provided by a set of 18 drift chambers with a total of 36 layers in each sector. Additional tracking at $5° - 35°$ is achieved by a set of 6 layers of micromesh gas detectors (micromegas) immediately downstream of the target area and in front of the High-Threshold Cherenkov counter (HTCC). Particle identification is provided by time-of-flight information from two layers of time-of-flight detectors (FTOF). Electron, photon, and neutron detection are provided by the triple layer electromagnetic calorimeter, PCAL, EC(inner), and EC(outer). The heavy gas Cherenkov Counter (LTCC) provides separation of high momentum pions from kaons and protons. The Central Detector consists of 6-8 layers of silicon strip detectors with stereo readout, 6 layers of micromegas, arranged as a barrel around the target, 48 scintillator bars to measure the particle flight time from the target (CTOF), and a central neutron detector. Further details on all CLAS12 components (magnets, detectors, data acquisition, software) may be obtained from Ref. [49].

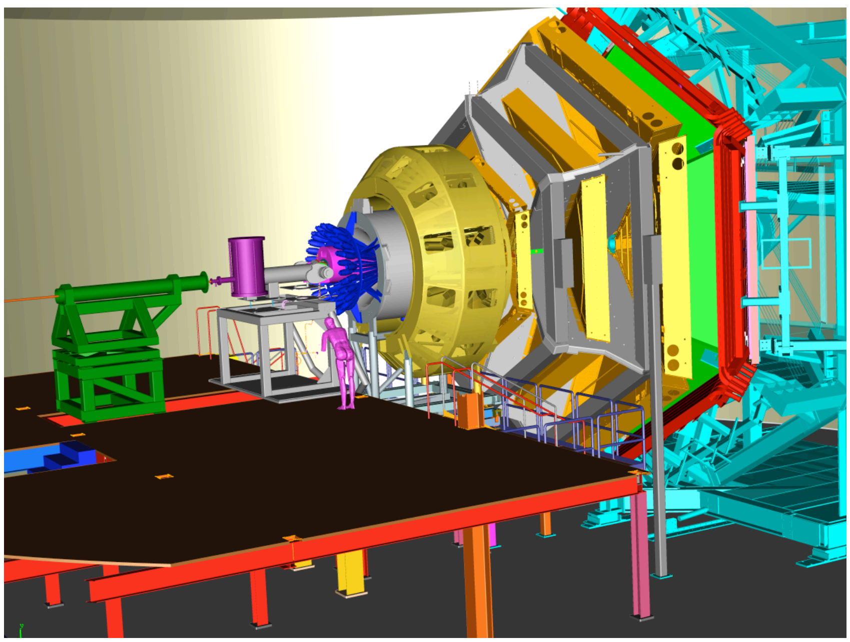

Figure 10: The CLAS12 detector has high hermeticity and high multiplicity reconstruction, can run at high luminosity ($L > 10^{35}\mathrm{cm}^{-2}\mathrm{s}^{-1}$), and is best suited to carry out the proposed experiment.

A polarized electron beam will be scattered off a liquid hydrogen target. The scattered electrons will be detected in the the Forward Detector of CLAS12 for scattering angles greater than about 6° and in Forward Tagger for angles from 2.5° to 4.5°, which allows us to cover the Q^2 range of interest between 0.05 and 2 GeV^2. Charged hadrons will be measured in the full range from 6° to 130°. At an operating luminosity of $L = 10^{35}$ cm^{-2}s^{-1} hadronic rates of 5×10^6 s^{-1} are expected.

4.2 The Forward Tagger

An essential component of the hadron spectroscopy program with CLAS12 is the Forward Tagger (FT) shown in Fig 11. The FT uses a high resolution crystal calorimeter composed of 324 lead-tungstate crystals to measure the scattered electrons in the polar angle range from 2.5° to 4.5° and with full coverage in azimuthal angle. The calorimeter measures electron and photon energies with an energy resolution of $\sigma(E)/E \leq 0.02/\sqrt{E(GeV)}+0.01$. The fine granularity of the calorimeter also provides good polar angle resolution. A two-layer tiled scintillator hodoscope is located in front of the calorimeter for the discrimination of photons. An additional four-layer micromegas tracker, located in front of the hodoscope, will be used for precise electron tracking information. Electron detection in the FT will allow us to probe the crucial Q^2 range where hybrid baryons may be identified due to their fast dropping $A_{1/2}(Q^2)$ amplitude and the suppression of the scalar $S_{1/2}(Q^2)$ amplitude. Construction of

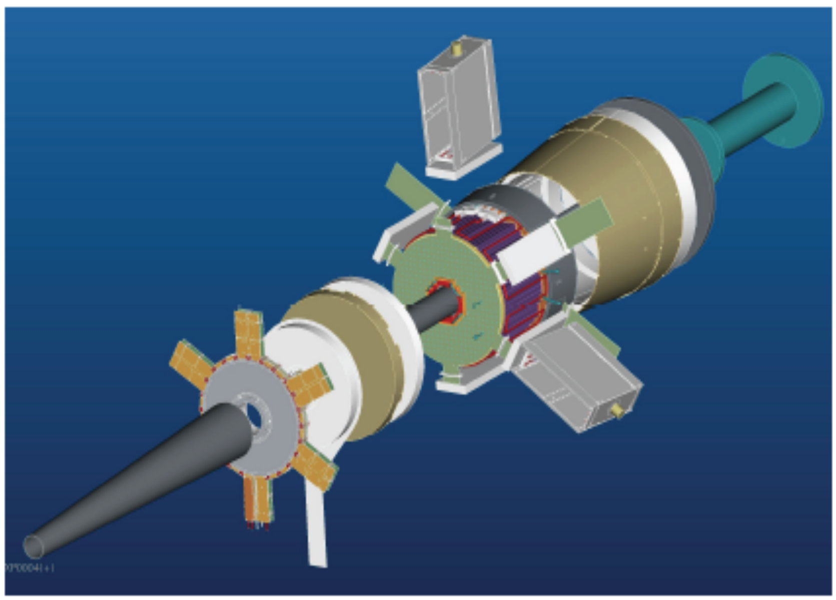

Figure 11: The Forward Tagger (FT) system. The FT provides electron and high energy photon detection in a range of polar angles $\theta_e = 2.5° - 4.5°$, and will be fully integrated into the operation of CLAS12.

the FT has been completed under the responsibility of INFN/Genova (Italy), CEA/Saclay (France), and the University of Edinburgh (UK). The FT has been shipped to Jefferson Lab, it has been assembled and it is now under calibration with cosmic rays. Installation into CLAS12 is expected in summer 2016.

4.3 Kinematical coverage of electron scattering in CLAS12

5 Simulations for the $ep \to ep\pi^+\pi^-$ final state

~~In order to account realistically for the acceptance of the processes we want to study, two event generators were developed for the processes $ep \to e'K^+Y$ (including either $ep \to e'K^+\Lambda$, followed by $\Lambda \to p\pi^-$ decay and $ep \to e'K^+\Sigma$, followed by $\Sigma \to \Lambda\gamma$ and $\Lambda \to p\pi^-$ decays) and $ep \to e'p\pi^+\pi^-$, respectively. Both reactions have four charged tracks in the final state and the event pattern coming from resonance decays may be quite similar. To the degree possible, the event generators have been tuned to existing data, mostly from CLAS. However, extrapolations to high W and very small Q^2 have been necessary, since no prior data exist. The generator for $ep \to e'p\pi^+\pi^-$ has been initially used to determine the most efficient configuration for beam energy and torus magnet setting in terms of field polarity and current.~~

5.1 Event generator for $ep \to ep\pi^+\pi^-$

~~The Monte Carlo simulation of the $\pi^+\pi^-p$ exclusive electroproduction was carried out in the range of invariant masses of the final hadron system W from the two-pion production threshold to 3 GeV and at photon virtualities Q^2 from 0.05 GeV^2 to 3.0 GeV^2.~~ The ~~established~~ previously existed 2π event generator was written in FORTRAN and had several limitations. It employed the $\pi^+\pi^-p$ differential cross sections from the older JM05 version of the JM model [46–48]. During the past several years the model was further developed [8] and significantly improved. Furthermore, the two-pion part of that event generator was only applicable up to 2 GeV in W and from 0.3 GeV^2 in Q^2, and therefore excluded most of the region of interest (high W and low Q^2), where it used simple interpolations. A substantial need to develop new event generator emerged, and it was successfully developed for this Proposal.

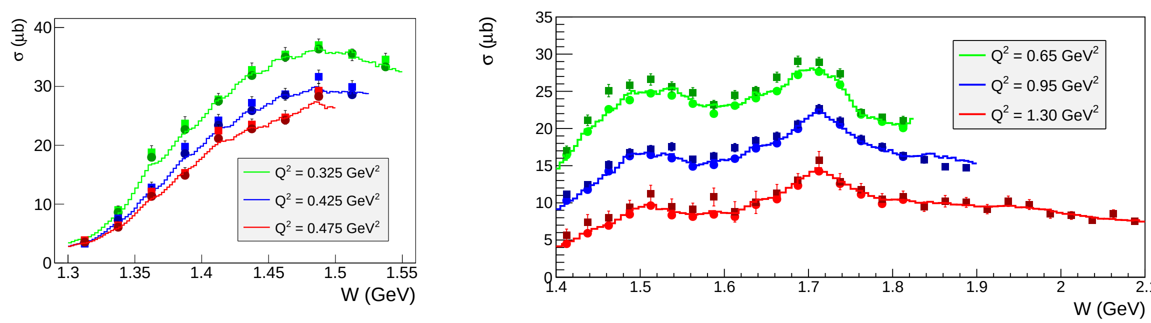

Figure 12: Comparison between the event distributions of the new two-pion event generator (curves) with the integrated cross sections from JM model (circles) and data (squares). Left plot shows the W dependence of the total cross section for three Q^2 bins in comparison with the model [51] and data [52] for the corresponding three Q^2 points at 0.325, 0.425, and 0.475 GeV^2. Right plot shows the W dependence of the total cross section for three Q^2 bins in comparison with the model [8] and data [50] for the corresponding three Q^2 points at 0.65, 0.95, and 1.3 GeV^2.

The new event generator employs the 5-fold differential cross sections from the recent

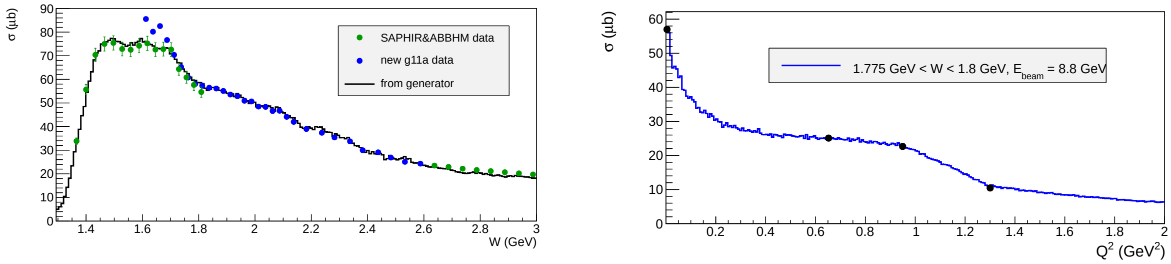

Figure 13: Left plot shows the W dependence of the integrated cross section for quasi-real Q^2 (0.0015 GeV^2) in comparison with data [53–55]. Right plot shows a typical example of Q^2 dependence of the total cross section for one W bin in comparison with JM15 [8] at $W = 1.7875$ GeV for 8.8 GeV electron beam energy.

version of the JM15 model fit to all results on charged double pion photo- and electroproduction cross sections from CLAS (both the published and preliminary [50–52, 55]). In the areas covered by CLAS data new event generator successfully reproduces the available integrated and single differential 2π cross sections. The quality of the description is illustrated in Fig. 12 for several Q^2 bins in comparison with the available electroporoduction data [50–52].

In order to extend event generator to the area not covered by CLAS data, a special extrapolation procedure was applied, that included additional available world data on W dependencies of 2π photoproduction integrated cross sections [53, 54]. The new approach allows to generate 2π events at extremely low Q^2 (less than 0.1 GeV^2) and high W (up to 3 GeV). On the left side of Fig. 13 the W dependence of integrated cross section for quasi-real Q^2 (0.0015 GeV^2) is shown in comparison with data [53–55]. The right side of Fig. 13 illustrates a typical example of Q^2 dependence of the total cross section for one W bin in comparison with JM15 [8] for 8.8 GeV electron beam energy.

The new event generator has more advantages: it generates phase space distributions and applies multidimensional cross section as a weight for each event. This method enables to significantly speed up the generation process, especially in the areas with sharp cross section dependencies. It makes also possible to obtain absolute values of cross section from the generated distributions and this is helpful for various additional purposes, such as cross section predictions in areas not covered by experiment.

The new 2π event generator is written in C++, it includes inclusive radiative effects according to the approach described in [56] and produces an output compatible with the new CLAS12 reconstruction software.

Studies of the run conditions for this Proposal were carried out with new 2π event generator described above. Exclusive events for $\pi^+\pi^-$ electroproduction off proton were generated in the range of invariant masses of the final hadron system W from the two-pion production threshold to 3 GeV and at photon virtualities Q^2 from 0.01 GeV^2 to 2.0 GeV^2 (see Fig. 14) .

5.2 Acceptance estimates for $ep \to ep\pi^+\pi^-$

For the event reconstruction a simplified version of the CLAS12 event reconstruction software, the so-called FASTMC routine, was employed to filter the generated events for acceptance. This routine accounts for the detector fiducial areas and provides smearing over the

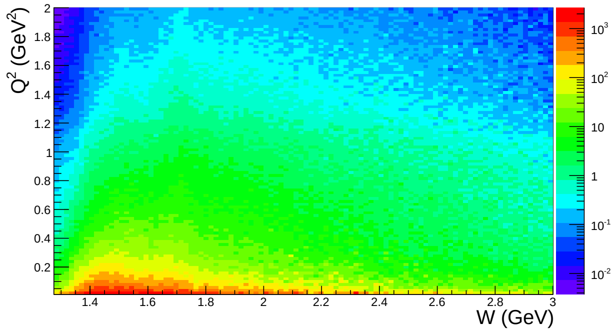

Figure 14: Q^2 versus W distribution for the generated $\pi^+\pi^-p$ events with an electron beam energy of 6.6 GeV.
~~The GENEV event generator based on JM05 was used to generate 10^6 events.~~

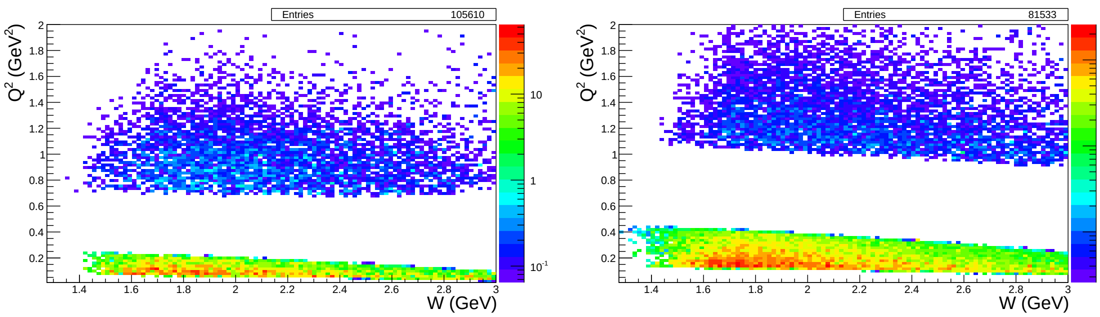

Figure 15: Q^2 versus W distributions for the reconstructed $\pi^+\pi^-p$ events (all particles in final state are registered). Left and right plots correspond to 6.6 GeV and 8.8 GeV beam energies, respectively. The torus current is set to + 3375 A.

final particle angles and momenta. The accepted events are shown in Fig. 15 and are plotted in the Q^2 versus W plane. Left and right panels show the distributions for the reconstructed $\pi^+\pi^-p$ events at two beam energies. The torus current was set to +3375 A, which forces negatively charged particles to bend towards the beam line. The areas of zero acceptance seen in the plots represent the gap between the Forward Tagger and the minimum polar angle accepted in CLAS12 for inbending particles. For the hybrid baryon search the area of small photon virtuality is of particular interest. The size of the gap depends on the torus current setting and the momentum of the scattered electrons. For a negative Torus current, i.e. outbending electrons, the gap is simply given by the geometrical acceptance of CLAS12 and is largely independent of the particle momentum, while for inbending particles the acceptance depends on scattering angle, particle momentum, and magnetic field strength. The acceptance for electron scattering angles from 2.5° to 4.5°, which is covered by the FT, is independent of the torus current settings. In order to cover photon virtualities as low as 0.05 GeV^2 measurements with 6.6 GeV electron beam energy are required. The minimal Q^2 values for reconstructed events increase up to 0.13 GeV^2 for beam energy of 8.8 GeV. A simulated $ep \to e'p\pi^+\pi^-$ event in CLAS12 is shown in Fig.18.

With a beam energy of 6.6 GeV, the influence of the magnetic field direction on the accessible kinematical coverage for $\pi^+\pi^-p$ electroproduction was further studied. The Q^2 versus W distributions for reconstructed $\pi^+\pi^-p$ events are shown in Fig. 16 for two opposite polarities of the torus current, +3375 A and -3375 A, which correspond to the maximum expected currents. A wide area of zero acceptance for the normal (+3375 A) direction of the magnetic field is clearly seen in Figure 16 (left). Reversing the magnetic field allows us to decrease substantially the inefficient area, as is shown in Fig. 16 (right). Therefore, the reversed magnetic field represents the best configuration for the proposed experiment, as well as for other experiments, for which the area of small photon virtualities is of particular interest.

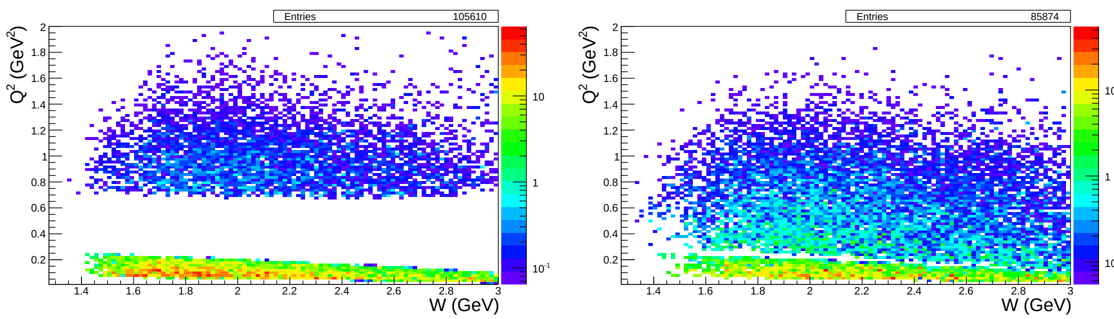

Figure 16: Q^2 versus W distributions for reconstructed $\pi^+\pi^-p$ events (all particles in final state are registered) for the torus currents +3375 A (left) and -3375 A (right). The reversed magnetic field closes the gap between the Forward Tagger and CLAS12.

We also examined the evolution of counting rates as a function of the magnetic field strength. The 2D Q^2 versus W distributions for the accepted $\pi^+\pi^-p$ events are shown in Fig. 17 for the torus currents, -3375 A (left) and -1500 A (right), that correspond to the full and less than half strength magnetic fields for the CLAS12 detector. Comparing the reconstructed event rates shown in Fig. 17, we expect the counting rate to increase by almost a factor of two at half strength of the magnetic field, because of the improved acceptance for the detection of all three $\pi^+\pi^-p$ particles in the final state and the scattered electron. From the other hand decreasing of the torus current will negatively affect particles momentum resolution. So, a compromise between this two factors is needed.

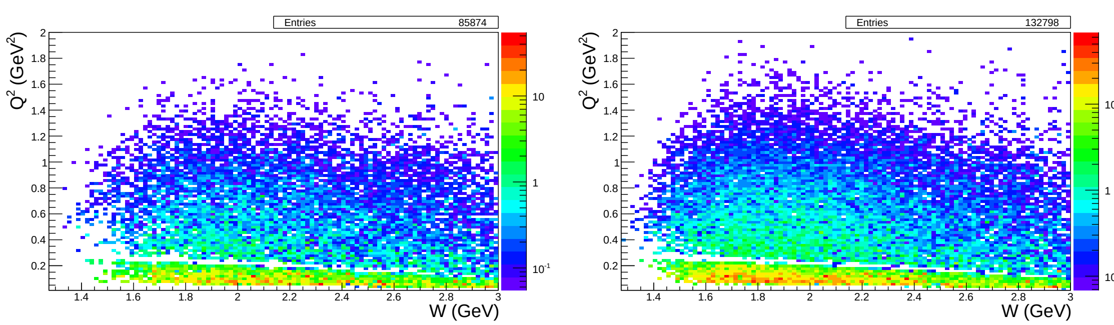

Figure 17: Q^2 versus W distributions for reconstructed $\pi^+\pi^-p$ events at 6.6 GeV beam energy (all final state particles are registered) with torus currents: -3375 A (left) and -1500 A (right). With lower torus current more events are reconstructed.

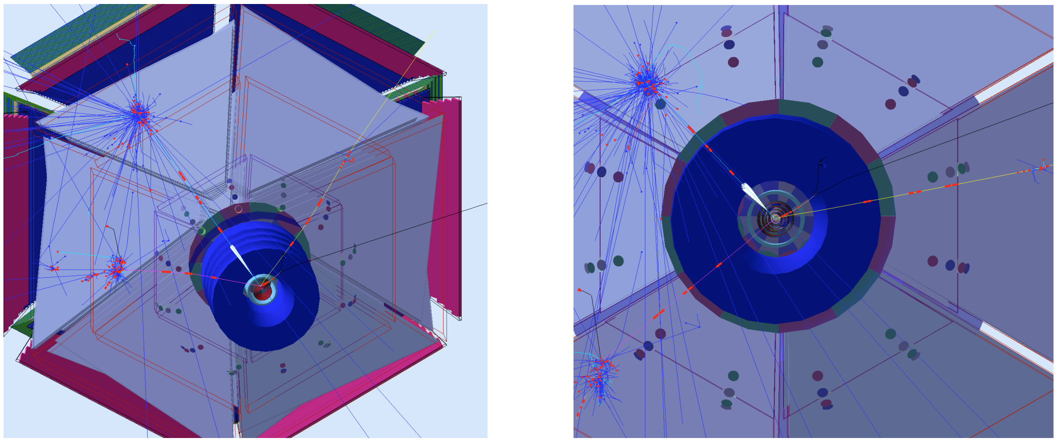

Figure 18: A Geant4 $ep \to ep\pi^+\pi^-$ event as seen in CLAS12. The left graph shows the scattered electron (cyan) generating Cherenkov light in the HTCC, leaving track segments in the 3 drift chamber regions, and hits in the FTOF planes and finally shower in the PCAL & EC calorimeters. The two pions π^+ (purple line) and π^- (yellow line) are tracked in the DCs, and leave hits in the FTOFs and calorimeters. The proton (short orange line) is tracked at large angles inside the solenoid magnet in the four SVT regions, and leaves hits in the CTOF. The right panel shows a close-up view of the same event from a different angle. The torus magnet is at 50% of full current.

5.3 Resolution in hadronic mass reconstruction and background estimation for $ep \to ep\pi^+\pi^-$

The hadronic mass resolution is of particular importance in studies of excited nucleon states, since this quantity determines the ability to reliably extract the resonant contributions in exclusive cross sections. For a credible separation between the resonant and the non-resonant contributions the resolution over W should be much smaller than the N* decay width. Typical values for the decay widths of nucleon resonances with masses > 2.0 GeV are in a range from 250 to 400 MeV. Hence a mass resolution of ≈ 30 MeV is sufficient for the reliable isolation of contributions from hybrid-baryons that are expected in the mass range from 2.0 to 3.0 GeV. The resolution in W for the reconstructed $\pi^+\pi^-p$ events was studied in the following way. For each reconstructed event we compute the difference between the exact W_{gen} and the reconstructed W_{rec}. We compare two different ways of determining the invariant mass of the final hadron system: a) from the difference between the four-momenta of the initial and the scattered electrons that is added to the four-momentum of the target proton (electron scattering kinematics) b) from the sum of the four-momenta of the final π^+, π^-, and proton (hadron kinematics). The reconstructed W_{gen} - W_{rec} event distributions provide the necessary information on the invariant mass resolution.

The aforementioned distributions for the electron scattering and hadron kinematics are shown in Fig. 19. The beam energy is set to 6.6 GeV and torus current to -1500 A. For both ways of determining the W_{rec} value, the resolution over the full W range is better than 30 MeV and sufficient for the separation of resonant/non-resonant contributions. If W_{rec} is computed from the hadron kinematics, the resolution is significantly better than in the case of electron scattering kinematics. However, the hadron kinematics requires the registration of all final hadrons with a detection efficiency lower than in the inclusive case where the value of W_{rec} is determined from the electron scattering kinematics.

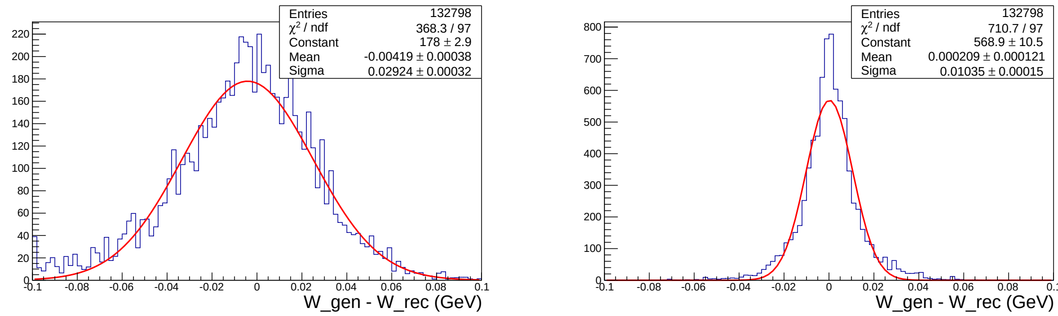

Figure 19: The $W_{gen} - W_{rec}$ distributions for $\pi^+\pi^-p$ events where W_{rec} is determined by electron scattering (left) and hadron (right) kinematics. See text for explanation of both kinematics.

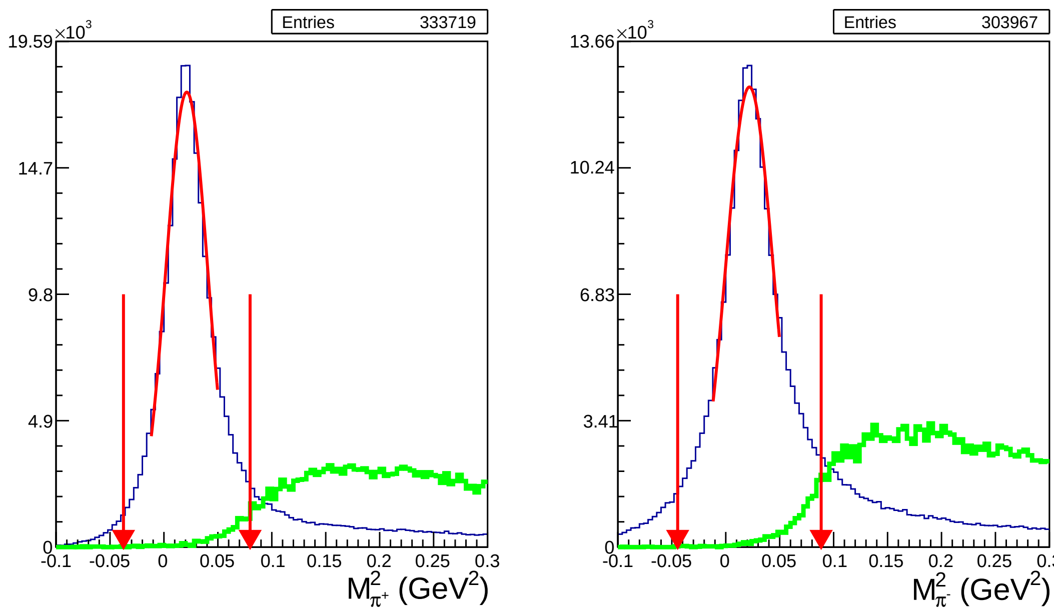

Figure 20: The reconstructed $\pi^+\pi^-p$ event distributions of the missing masses squared of π^+ (left) and π^- (right) for the generated $\pi^+\pi^-p$ events with an admixture of 3π events. The distributios were plotted for $W > 2$ GeV. Cross sections of 2π and 3π channels were assumed comparable in this kinematic region. The contributions from the $\pi^+\pi^-p$ and the $\pi^+\pi^-\pi^0p$ events are shown in blue and green, respectively. The red arrows indicate the applied exclusivity cuts.
~~The reconstructed $\pi^+\pi^-p$ event distributions of the missing masses squared of π^+ (left) and π^- (right) for the generated $\pi^+\pi^-p$ events with an admixture of 9% from 3π events. The contributions from the $\pi^+\pi^-p$ and the $\pi^+\pi^-\pi^0p$ events are shown in blue and green, respectively. The red arrows indicate the applied exclusivity cuts.~~

The studies of charged double pion electroproduction with the CLAS detector [50, 52]

Energy (GeV)	Torus current (A)	Eff. all reg. (%)	Eff. π^+ miss (%)	Eff. π^- miss(%)	Eff. proton miss(%)	Q^2_{min} (GeV^2)	σ(W) (GeV)	$\sigma(\sqrt{s})$ (GeV)
8.8	+3375	8.2	9.8	10.3	8.6	0.13	35	11
8.8	**-3375**	**8.3**	**12.7**	**10.6**	**12.1**	**0.13**	**33**	**10**
8.8	+1500	11.5	12.9	11.9	11.6	0.13	35	11
8.8	-1500	12.8	16.8	13.5	16.0	0.13	36	11
6.6	+3375	10.6	13.0	14.1	11.4	0.05	27	11
6.6	**-3375**	**8.7**	**13.8**	**11.5**	**13.1**	**0.05**	**26**	**10**
6.6	+1500	15.0	17.3	16.3	15.7	0.05	25	11
6.6	-1500	13.4	18.4	14.8	17.7	0.05	29	10

Table 1: Comparison of run conditions for the $\pi^+\pi^-p$ channel. Bold rows represent the optimal run conditions for 6.6 and 8.8 GeV beam energy runs.

demonstrated that the topology, where the final π^- is not detected and its four-momentum is reconstructed from energy-momentum conservation, provides the dominant part of the statistics. Hence topologies in which one of the final hadrons is not detected will provide the dominant statistics also in the proposed experiment. We are planning to select the $\pi^+\pi^-p$ events by employing exclusivity cuts on the missing mass squared distributions of any of the final hadrons. The contribution from other exclusive channels (exclusive background) to the events within the exclusivity cuts was evaluated in the Monte-Carlo simulation. Most of the exclusive background events come from the $ep \to e'p'\pi^+\pi^-\pi^0$ channel. Both $\pi^+\pi^-p$ and ~~3π~~ $\pi^+\pi^-\pi^0p$ events were generated for $W > 2$ GeV. Cross sections of 2π and 3π channels were assumed comparable in this kinematic region. ~~with a relative contribution from 3π events of $\approx 9\%$~~. A phase space distribution is assumed for the 3π events. With this mixture of generated events we reconstructed the $\pi^+\pi^-p$ events and determined their distribution over the missing mass squared for π^+ and π^-. They are plotted in Fig. 20. The blue curves in Fig. 20 show the 2π event contributions and the green curves represent the 3π event contributions. The exclusivity cuts provide ~~excellent~~ good isolation of the $\pi^+\pi^-p$ events with ~~almost negligible (less than 1%) contribution~~ the following contributions from the 3π events: about 3% for π^+ missing topology and 4% for π^- missing topology.

5.4 Summary of experimental conditions study

The summary of the run conditions studied in the simulations described above is listed in Table 1. Bold rows correspond to the optimal set-up for the proposed experiment.

Whereas the summary of the kinematical coverage in terms of 2D plots of ϕ versus θ distributions for the final hadrons is shown in Fig. 21 for all final hadrons detected, a beam energy of 6.6 GeV, and torus current -1500 A. The vertical strips at $\theta = 40°$ in all plots of Fig. 21 correspond to the detector gap between forward and central parts of CLAS12. Since a reversed torus magnetic field was chosen, the low angle area is better populated for negatively charged particles (π^-).

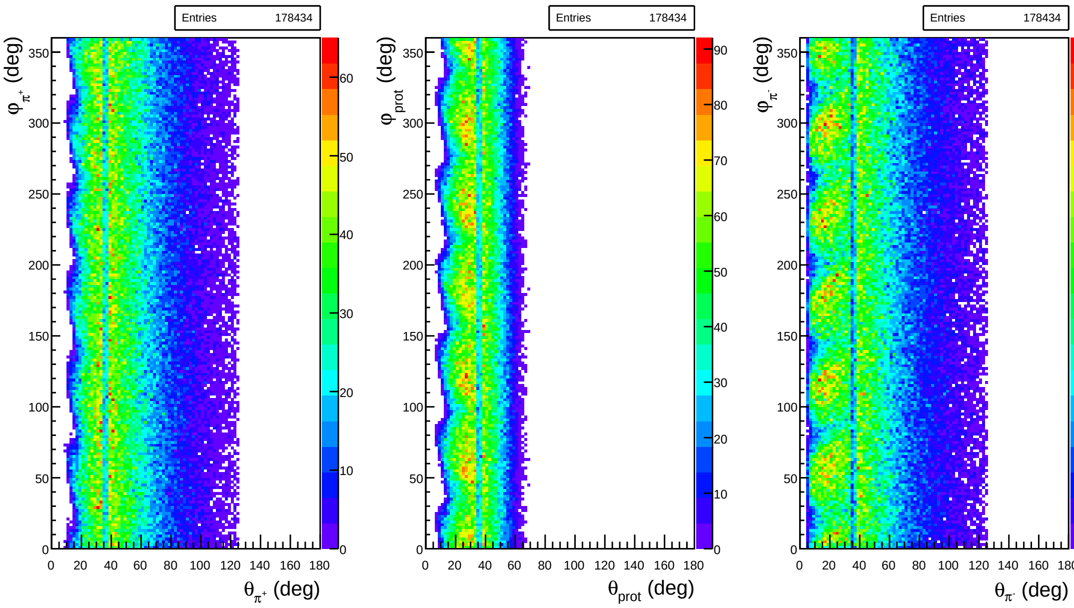

Figure 21: φ vs θ distributions for the final hadrons: π^+ (left), proton (middle), and π^- (right).

6 Simulations for the $K\Lambda$ and $K\Sigma^0$ final states

6.1 The $K\Lambda$ and $K\Sigma^0$ event generator

The $ep \to e'K^+\Lambda$ event generator is based on model cross section calculations. The models [9] for the $K^+\Lambda$ and [57] for the $K^+\Sigma^0$ channels describe KY electroproduction in the framework of a Regge-plus-resonance approach. Resonance contributions in the s-channel are described with the help of the effective-Lagrangian approach and the background part of the amplitude is modeled in terms of t-channel Regge-trajectory exchange.

A comparison of the fully integrated model cross section with experimental CLAS data is shown in Fig. 22. The cross sections are presented as a function of Q^2 for a given bin in $W = 2.05$ GeV. Differential cross sections in certain bins of Q^2 and W are shown in Figs. 23 and 24. The model reproduces the experimental data for 0.65 GeV^2 < Q^2 < 1.5 GeV^2, while it considerably underestimates the cross section for $Q^2 > 1.5$ GeV^2. This underestimation is especially notable in the $K^+\Sigma^\circ$ channel for high Q^2 and low W, see plot corresponding to $Q^2 = 1.8$ GeV^2 and $W = 1.73$ GeV in Fig. 24. It does not create any problems since our region of interest is at low Q^2. We have to rely on the model cross section for $Q^2 < 0.65$ GeV^2, as there are no experimental data to compare to. We can see in Figs. 23 and 24 that the model reproduces well the general features of the sharp cross section growth at large $\cos(\theta)$ for $Q^2 > 1.5$ GeV^2 and $W > 2.0$ GeV.

6.2 Acceptances for $ep \to e'pK^+\Lambda$

In Figs. 25 and 26 we compare the angular distributions of all final states particles for an electron beam of 6.6 GeV and for torus currents of +1500 A and the -1500 A. In Fig. 25 (should we change the figures plots with plus-minus 3370 torus configurations?) we see qualitatively the same behavior as for the $p\pi^+\pi^-$ final state: inbending electrons generated in a W interval from $K^+\Lambda$ threshold at 1.6 GeV to 3.5 GeV and scattering angles $\theta_e \geq 2^\circ$ are detected in CLAS12 starting at about 6.5° with the acceptance opening up towards larger scattering angles. The swirly pattern seen in the accepted protons and K^+ is due to the azimuthal motion of charged tracks in the strong solenoid field that generates a "kick" in azimuth that depends on the production angle and the particle momentum. It should be noted that the particles are not traversing the sectors in this pattern, as the plotted quantities are the values at the production vertex. The pattern for the π^- is different as they have on average much lower momenta and their migration in ϕ is larger and more diffuse. For KY production off hydrogen, the recoil protons are kinematically limited to polar angles of $\leq 65^\circ$. Figure 26 shows the acceptances for out-bending electrons for which the polar angle gap between the FT and CLAS12 is strongly reduced and the azimuthal response is more uniform. As a result, the event acceptance for this configuration is almost a factor 2 larger than for the in-bending field configuration. We also note that for both configurations there exists a polar-angle band from 35° to 40° where the acceptance is depleted due to the partially blind transition region between the forward and central detectors.

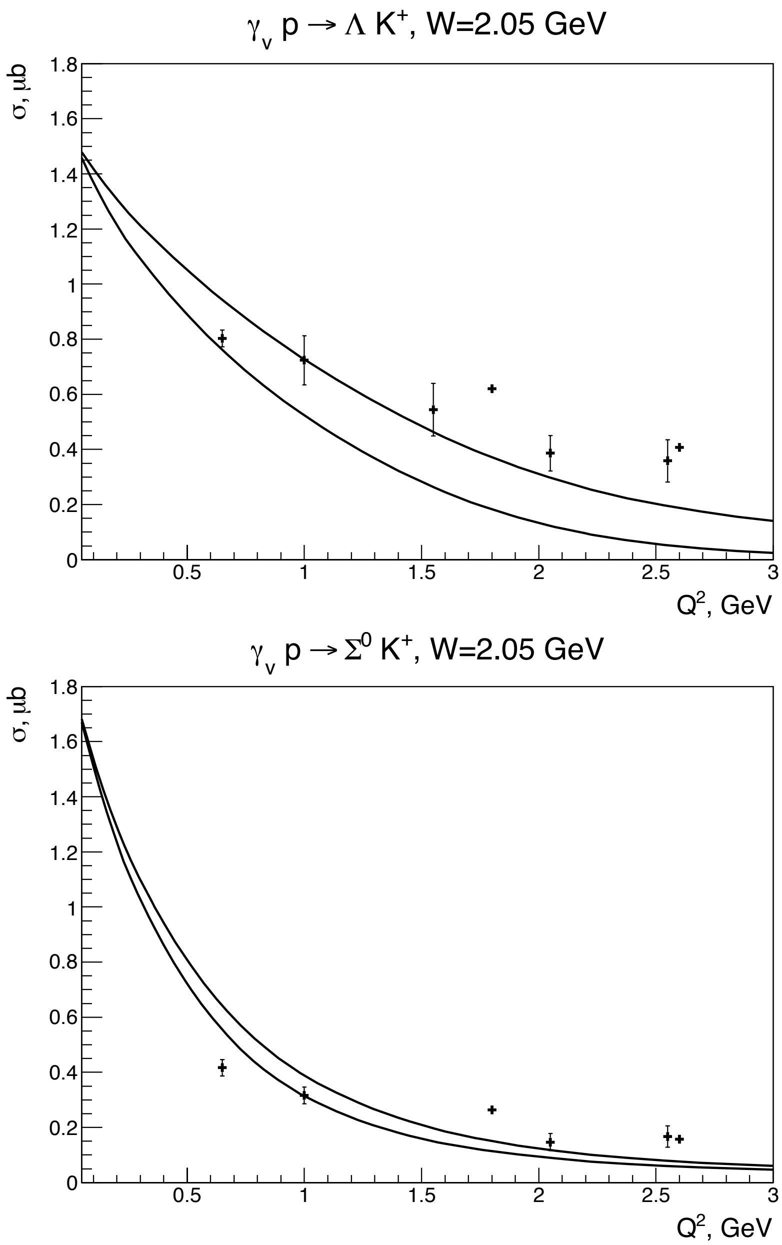

Figure 22: Integrated cross section for $K^+\Lambda$ (top) and $K^+\Sigma$ (bottom) as a function of Q^2 at $W = 2.05$ GeV. Experimental cross sections at $Q^2 = 0.65$ GeV^2 are measured at a beam energy of 2.567 GeV. Whereas cross sections at $Q^2 = 1.8$ GeV^2 and 2.6 GeV^2 are measured at a beam energy of 5.5 GeV. All other Q^2 points correspond to a beam energy of 4.056 GeV. Model calculations are shown in two curves: upper curve is for a beam energy of 2.567 GeV and lower for 5.5 GeV.

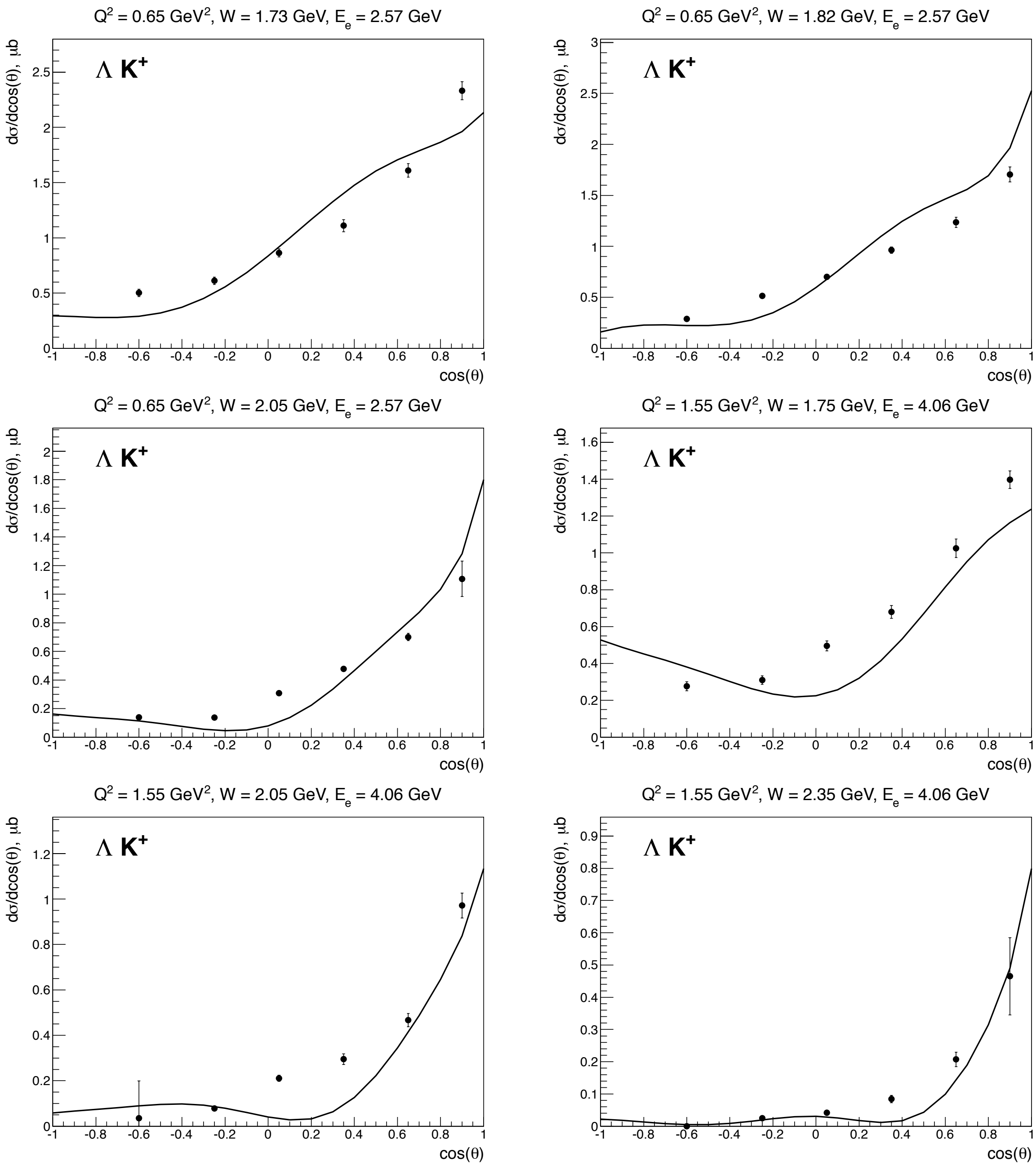

Figure 23: Differential cross sections for $K^+\Lambda$ channel in various Q^2, W bins for two different beam energies. θ is the polar angle of the kaon in the CMS.

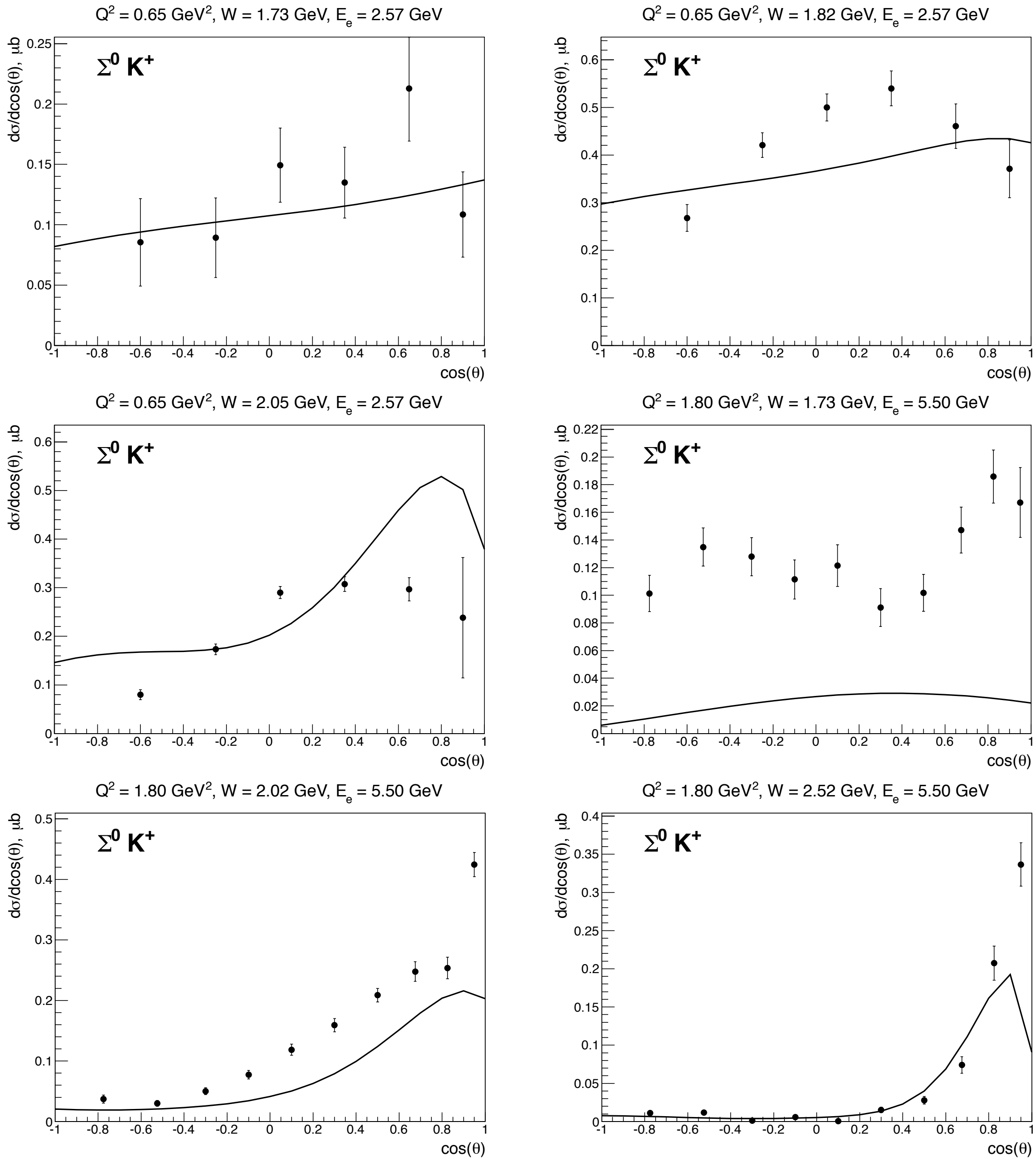

Figure 24: Differential cross sections for for $K^{+}\Sigma^{\circ}$ channel in various bins of Q^2, W bins for some beam energies. θ is polar angle of the kaon in CMS.

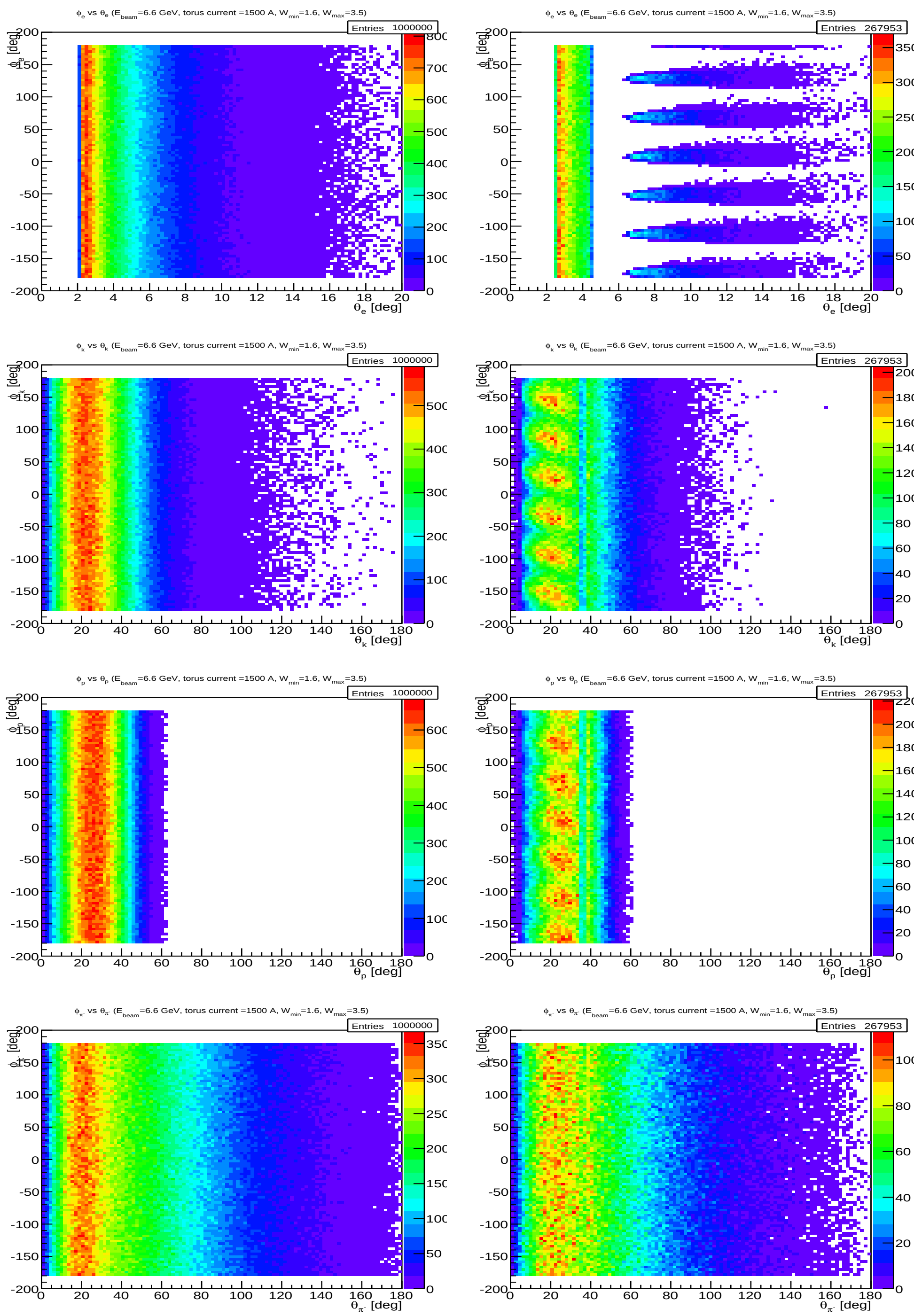

Figure 25: Azimuthal versus polar angle of generated (left) and accepted events (right) for electrons (top row), K^+ (2nd row), protons (third row), and π^- (bottom row). Events are generated for an electron beam energy of 6.6 GeV in a W range from 1.6 to 3.5 GeV. The torus current is set I=+1500A, that bends negatively charged particles inward towards the beamline and reduces the acceptance for electrons within CLAS12.

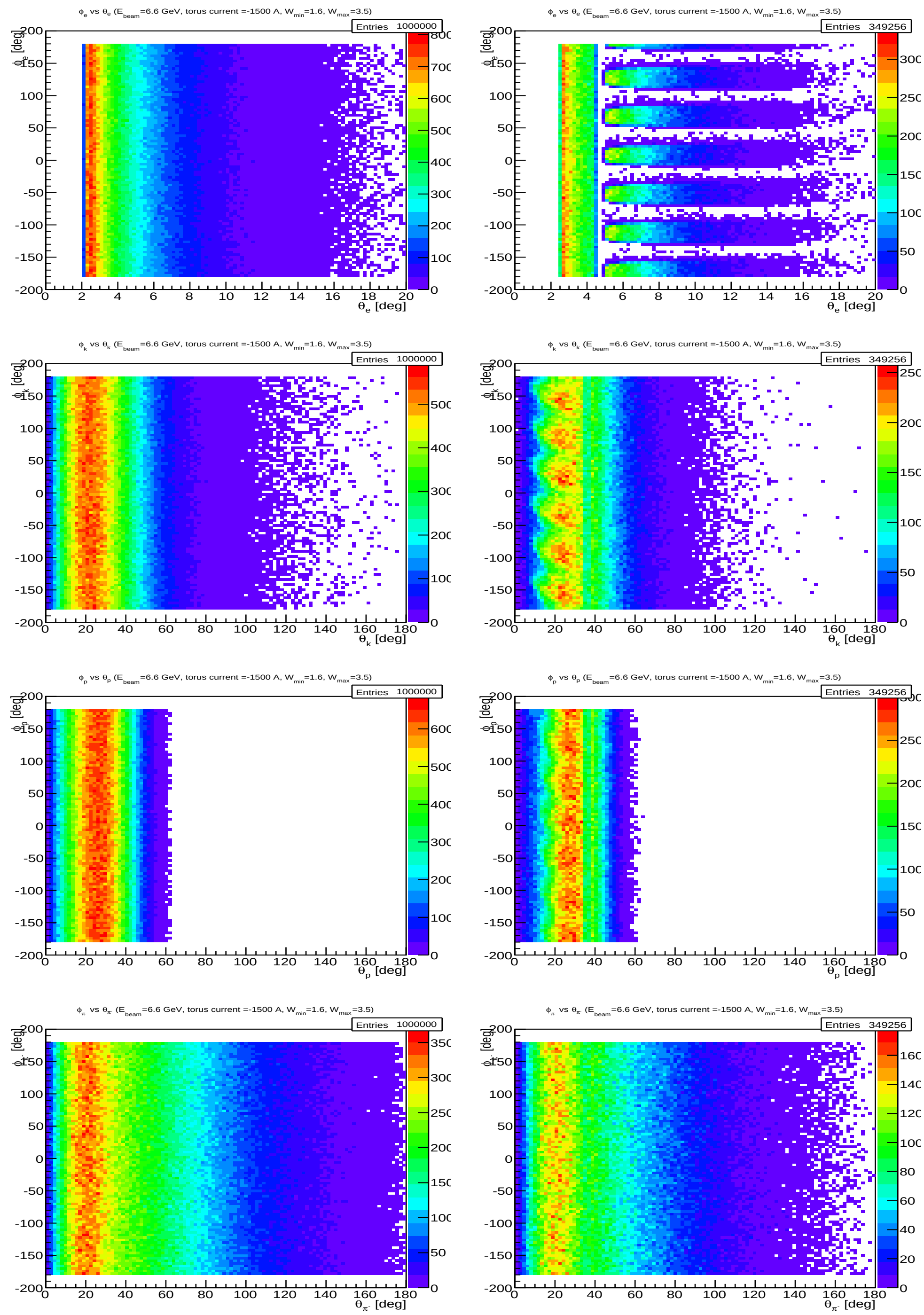

Figure 26: Azimuthal versus polar angle of generated (left) and accepted events (right) for electrons (top row), K^+ (2nd row), protons (third row), and π^- (bottom row). Events are generated for an electron beam energy of 6.6 GeV in a W range from 1.6 to 3.5 GeV. The torus current is set at I=-1500A, that causes negatively charged particles to bend outwards.

6.3 Run conditions

We are planning to search for the hybrid states at low Q^2 and the accessible range of Q^2 depends on the beam energy and torus current. Another issue that affects the selection of the best run conditions is that we need good particle momentum resolution to be able to separate Λ and Σ^0 electroproduction channels and the best resolution is achieved with larger torus currents. The Λ and Σ^0 separation is based on using cuts on the reconstructed kaon missing mass. For this purpose the final kaon must be detected. Thus, we have to use the topologies where the final state electron, the kaon and at least one of the other hadrons (p or π^+) are detected.

The run condition studies were performed with fact MC. The results are shown in Figs. 27 and 28. Table 2 summarizes the relevant information for different run conditions. The best run conditions correspond to the large negative torus currents, as the maximal Λ and Σ^0 separation is achieved and the gap in the Q^2 coverage is small.

Table 2: Minimal achievable Q^2 (Q^2_{min}) and the percentage of the Λ and Σ^+ events that can be isolated from each other at different run conditions.

E_{beam}, GeV	Tor. current, A	Q^2_{min}, GeV^2	Λ separation, %	Σ^0 separation, %
6.6	+1500	0.05	33	19
6.6	−1500	0.05	86	73
6.6	+3700	0.05	32	19
6.6	**−3700**	0.05	100	100
8.8	+1500	0.1	21	8
8.8	−1500	0.1	31	16
8.8	+3700	0.1	16	8
8.8	**−3700**	0.1	100	100

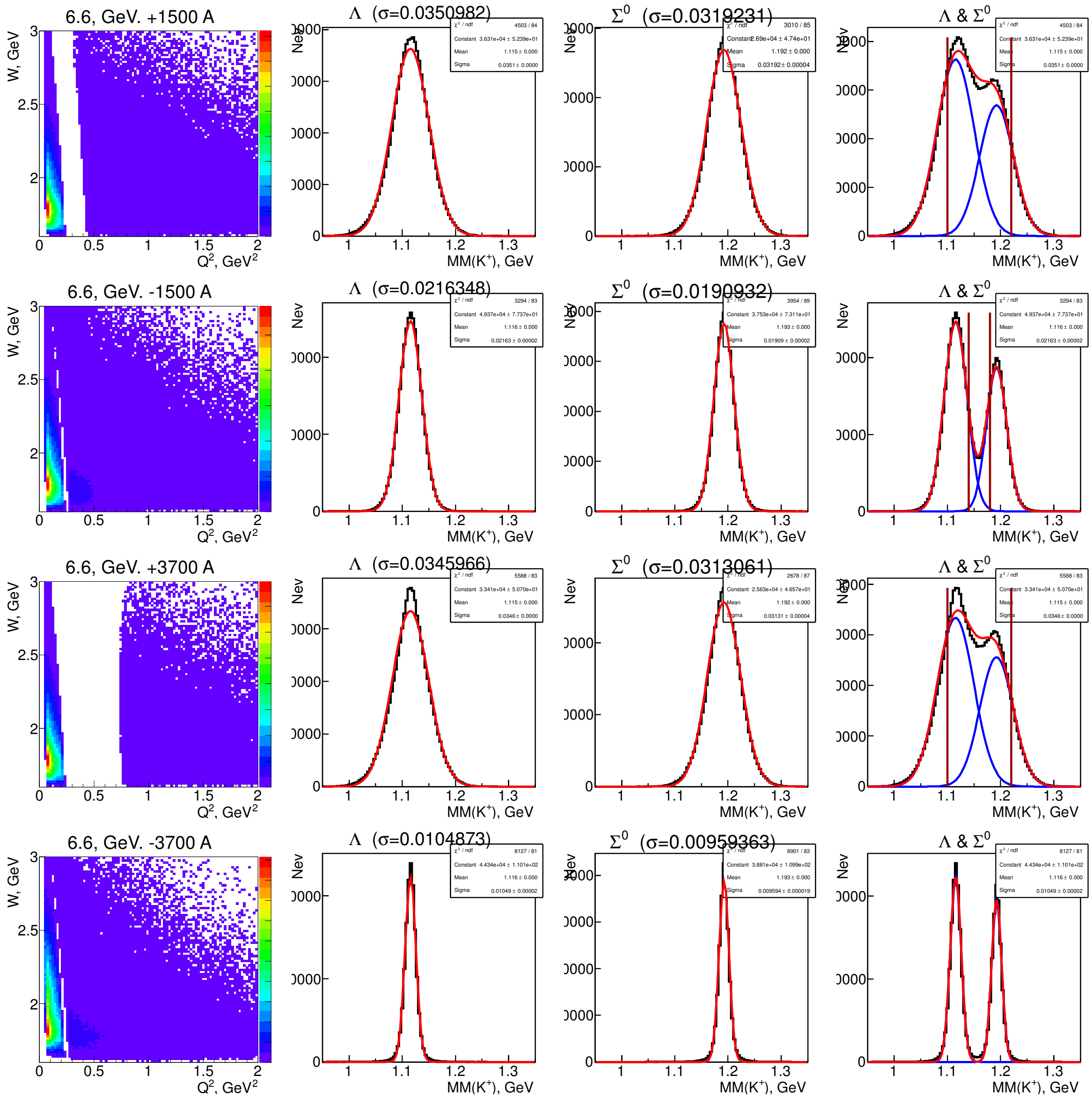

Figure 27: The left column shows the W versus Q^2 distributions at different torus currents for $Q^2 < 2$ GeV^2 when the beam energy is 6.6 GeV. Next three columns show the distributions of the missing mass off K^+ for the corresponding torus current. The vertical lines indicate the cuts to be used to separate Λ or Σ^0 from its neighboring state. When no lines are drawn then Λ and Σ^0 are fully separated.

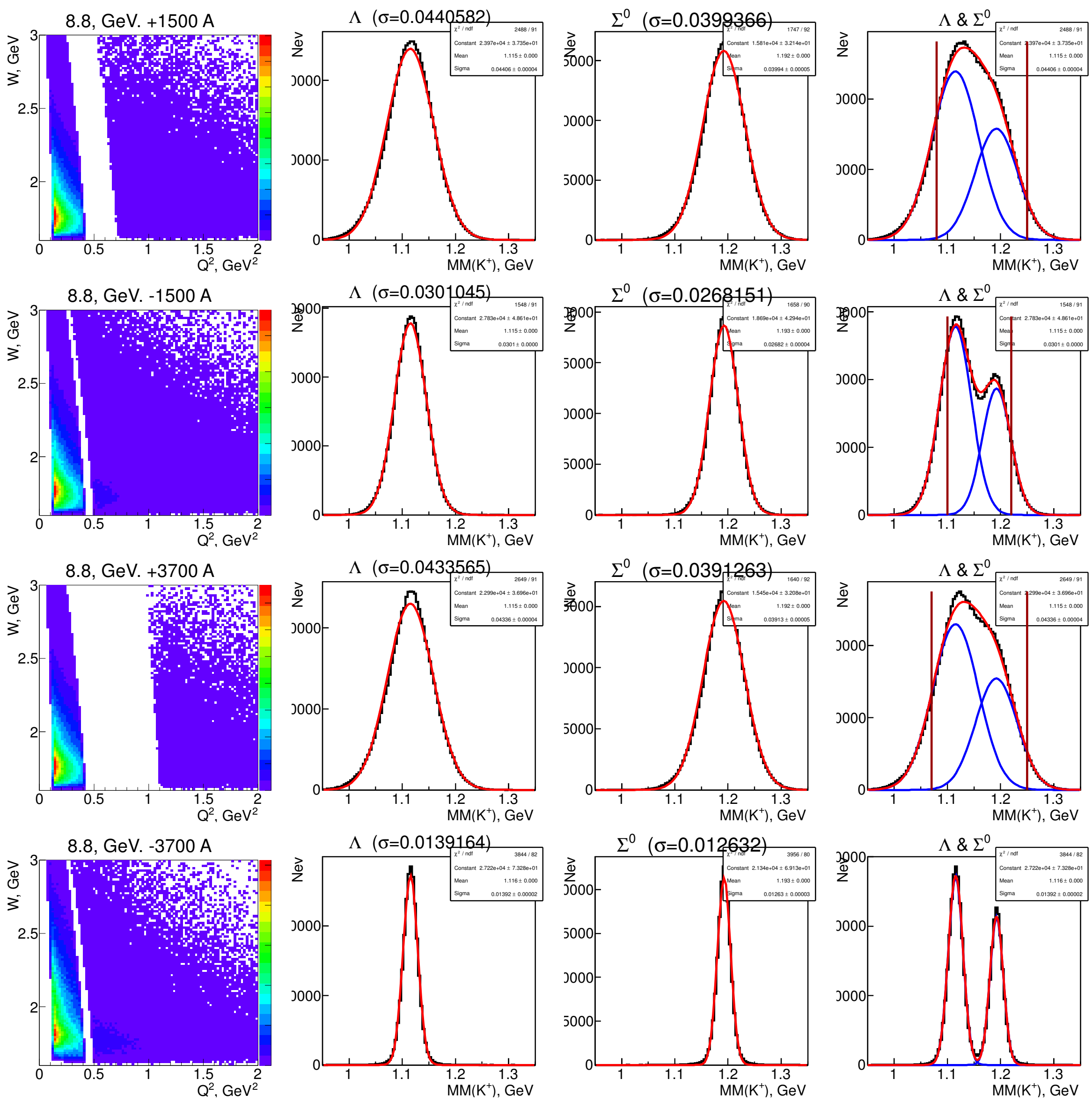

Figure 28: The left column shows the W versus Q^2 distributions at different torus currents for $Q^2 < 2$ GeV^2 when the beam energy is 8.8 GeV. Next three columns show the distributions of the missing mass off K^+ for the corresponding torus current. The vertical lines indicate the cuts to be used to separate Λ or Σ^0 from its neighboring state. When no lines are drawn then Λ and Σ^0 are fully separated.

6.4 Count rates from $K^+\Lambda$

The expected total number of KY electroproduction events in the reaction $ep \to eK^+Y$ can be written as:

$$N = L \cdot t \cdot \int \frac{d^5\sigma}{dE_e d\Omega_e d\Omega_K^*} dE_e d\Omega_e d\Omega_K^* \,, \tag{11}$$

where

- $L = 1 \times 10^{35}\,\mathrm{cm}^{-2}\mathrm{s}^{-1}$ is the expected CLAS12 operating luminosity
- t is the expected run time, and
- $\frac{d^5\sigma}{dE_e d\Omega_e d\Omega_K^*}$ is the cross section from (19).

Integration in (11) is performed over the whole kinematic space. The event rate R is defined as $\frac{N}{t}$.

Integration in (11) can be done numerically. We use the same model cross sections for $d^2\sigma/d\Omega_K^*$ as was used in the event generator (see section 6.1). The minimum achievable value of Q^2 in CLAS12 is determined by the forward hole, where high energy electrons cannot be detected. For all beam energies Q^2 is greater than 0.01 GeV^2, so we can integrate in (11) given that $Q^2 > 0.01$ GeV^2. The calculated event rates R_Λ and R_{Σ^0} are presented in Table 3.

Table 3: Estimated production rates for events with $Q^2 > 0.01$ GeV^2.

E_{beam}, GeV	R_Λ, Hz	R_{Σ^0}, Hz
6.6	1500	1200
8.8	1400	1100

To account for the acceptance of CLAS12 a detailed simulation is needed. As we need to generate events in the whole kinematic space with $Q^2 > 0.01$ GeV^2, the ratio of reconstructed to generated events gives the averaged acceptance. Multiplying the event rates from Table 3 by that ratio gives us event rates which account for the acceptance.

An $ep \to e'K^+\Lambda \to e'K^+p\pi^-$ event is considered to be reconstructed, if the electron and at least two hadrons have been detected. A trigger condition requiring at least two charged hadrons and an electron would select our channels of interest. Production rate calculations are presented in Table 4 for all possible beam energies and torus currents. Currently FASTMC is used to estimate the acceptance. A full simulation and reconstruction will be carried out in the near future. the following table should already take into account the $\Lambda \to p\pi^-$ BR: ie numbers should be multiplied by 0.64

A rough estimate suggests that the KY exclusive channel contribution is about 1% with respect to the two and three pion production, which are expected to dominate the statistics of events that have an electron and at least two charged hadrons in the final state. The maximal total event rate is therefore expected to be 240x100 = 24 kHz for the trigger condition described above. The count rate also can be estimated in the following

Table 4: Estimated and acceptance reduced event rates for the channel $ep \to eK^+\Lambda \to eK^+p\pi^-$. Electron and two hadrons are required to be accepted.

E_{beam}, GeV	Torr. cur, A	R_Λ, Hz
6.6	+1500	225
6.6	−1500	240
6.6	+2950	135
6.6	−2950	112
8.8	+1500	168
8.8	−1500	168
8.8	+2950	105
8.8	−2950	82

way. Suppose, the maximal inclusive event rate is 20 KHz, which is limited by the data acquisition. Then under the rough assumption that Λ event rate is about 1% with respect to the inclusive event rate, we can estimate the Λ event rate to be $\approx$ 200 Hz. This number is in a reasonable coincidence with the previously obtained value of 240 Hz.

However, the studies in the section 6.3 showed that the preferable run conditions are achieved when using large negative torus currents, as Λ and Σ^0 can be fully separated.

The rate of the "separated" Λ or Σ^0 events when the beam energy is 6.6 GeV and the torus current is -1500 A is expected to be 240 Hz $\times$ 86% $\approx$ 200 Hz (see section 6.3). When the beam energy is 6.6 GeV and the torus current is -2950 A the same rate is 112 Hz $\times$ 100% $\approx$ 100 Hz. However, we have to take into account: first the total event rate of 24 kHz may not be feasible due to the limitations of the data acquisition and secondly the momentum resolution may differ from what is predicted by fast MC, and in this case the percentage of the separated Λ or Σ^0 events may become smaller.

The obtained event rate should be reduced by 8%, as this is the fraction of events that do not have a reconstructed kaon (isn't this already taken into account by the acceptance?) (to be removed: and by 34%, since the Λ decay branching fraction to the channel (p, π^-) is 64%). Assuming the Λ electroproduction detection rate is 64 Hz (to be removed: 100 Hz), in 30 days of the beam time we expect to collect 64 Hz $\times$ 0.92 $\times$ 30 days $\approx 1.5 \times 10^8$ events (to be removed: 100 Hz $\times$ 34% $\times$ 64% $\times$ 30 days $\approx 1.5 \times 10^8$ events).

6.5 Expected total event rates

At the very forward electron scattering angles, electron rates will be very high and may exceed the capabilities of the data acquisition system. Therefore additional constraints are needed to define an optimal trigger configuration, which would enrich the sample with final state topologies as one might expect them from hybrid baryon candidates and reduce the total acquisition rate. For an initial program we therefore consider to trigger on hadronic final states with at least two charged particles. This will cover final states: $K^+\Lambda \to K^+p\pi^-$, $p\pi^+\pi^-$, $p\phi \to pK^+K^-$, $p\eta' \to p\pi^+\pi^-\eta$. For realistic rate estimates, projections of hadronic coupling strengths of hybrid baryons are needed, which are currently not available. In addition, a single charged hadron trigger will be incorporated with a pre-scaling factor for the FT that will in parallel collect events with a single charged hadron in the final state, i.e. π^+n, $p\pi^\circ$, $K^+\Lambda$, and $K^+\Lambda$, among others.

The operating luminosity of CLAS12 is estimated at $L = 10^{35}$ cm^{2}sec^{-1}. This corresponds to a production rate of 240 Hz (for $K^+\Lambda$) and about 170 Hz (for $K^+\Sigma^\circ$). For a 30 day run at that luminosity, the total number of $K^+\Lambda$ events is estimated at 1.2×10^9, and the number of $K^+\Sigma^\circ$ events at 0.85×10^9. The number of events in any histogram for certain smaller intervals of Q^2 and W can be found in the same way. The lowest event rate is expected for high Q^2 and high W. For the kinematics with lowest statistics, e.g. $2.0 \le Q^2 \le 2.5$ GeV^2 and $2.675 \le W \le 2.700$ GeV, a total number of 2.0×10^5 $K^+\Lambda$ events and 1.1×10^5 $K^+\Sigma^\circ$ events are expected.(to be checked)

While these rates seem very large, it should be kept in mind that the signals of hybrid baryons that we want to detect and quantify may be one or two orders of magnitude smaller than the signal from ordinary baryon states and will likely not simply be seen as a peak in the excitation spectrum, but rather as a broad region in W where specific quantum numbers, i.e. $I = \frac{1}{2}$ and $J^P = \frac{1}{2}^+$ or $J^P = \frac{3}{2}^+$, must be identified and the electromagnetic couplings must be measured versus Q^2. This can be achieved in a partial-wave analysis that includes other channels in a multichannel fit, such as the Bonn-Gatchina or Jülich/GWU approaches. Other techniques may also be employed. Very high statistics is thus essential, and the transverse and longitudinal photon polarization that is inherent in electron scattering will provide amplitude interference and enhance the resonant signal.

7 Data Analysis and quasi data

7.1 Event selection

Electrons will be detected both in the Forward Tagger and in the CLAS12 Forward Detector (FD). Electrons measured in the FD can be identified at scattering angles above 6° in the High-Threshold Cherenkov counter (HTCC) and in the PCAL and EC calorimeters. Due to the higher Q^2 for electrons detected at larger scattering angles in CLAS12 compared to the FT region, the FD electron rate is comparatively much lower than the hadronic rate, which ensures good electron identification.

For electrons detected in the FT, the low Q^2 leads to a very high electron rate that completely dominates the event rate in the FT calorimeter and hodoscope. A direct electron identification at the trigger level is therefore not needed. However the complete event pattern may be checked for consistency with that hypothesis in the event reconstruction. Note that the full electron kinematics is measured in the FT calorimeter and the micromegas tracker and charged particle ID is provided by the two layer hodoscope in front of the calorimeter as well as with hits in the micromegas tracker.

Charged hadrons ($\pi^\pm$, $K^\pm$, and protons) will be tracked in the drift chambers and micromegas in the FD, and in the silicon tracker and barrel micromegas at large angles in the CD. At all angles, charged particle identification is provided in the CLAS12 time-of-flight detector systems. Photons and neutrons are detected at forward angles in the electromagnetic calorimeters (PCAL, EC, FT) and neutrons at large angles are detected in the Central Neutron Detector (CDN).

7.2 Event reconstruction

The event reconstruction software has been designed and developed to be deployed within the ClaRA framework, a Service Oriented Architecture framework for data processing. The reconstruction application consists of a chain of services which can be deployed within ClaRA. The services for each detector component are compiled as java archive (JAR) plugins which are included in the complete CLAS12 Software release package coatjava. The CLAS12 reconstruction software reconstructs, on an event-by-event basis, the raw data coming from either simulation or the detectors to provide physics analysis output such as track parameters and particle identification. The package provides scripts that can be launched on the farm to cook the data as well as a framework to do event analysis using the flexible scripting language Groovy. The documentation for the coatjava package can available on the CLAS12 webpage: http://clasweb.jlab.org/clas12offline/docs/software/html/. For acceptance and efficiency studies, events are generated using the Geant-4 Monte Carlo simulation application GEMC. A detailed documentation of the detectors included in the simulation and of the various settings used to set the simulation parameters according to physics, backgrounds and magnetic field configurations is available from the gemc webpage: https://gemc.jlab.org/gemc/Documentation/Documentation.html. An example of a simulated event for the reaction $ep \to e'K\Lambda$ is shown in Fig. 29.

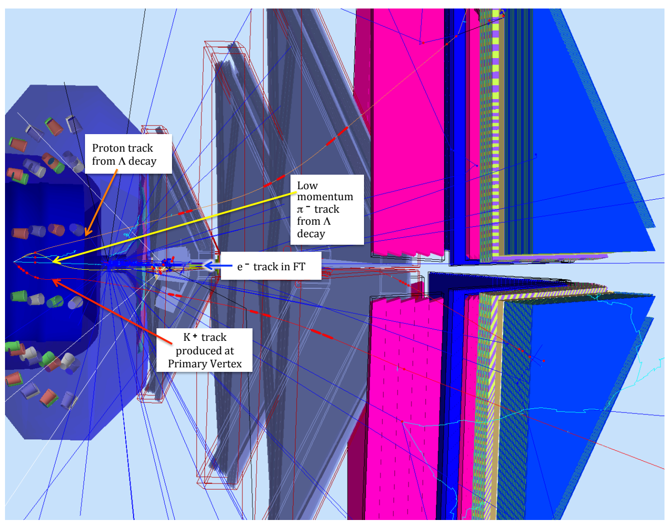

Figure 29: GEMC - Graphical User Interface Display of $ep \to eK^+\Lambda$ ($\Lambda \to p\pi^-$) event as seen in CLAS12 detectors.

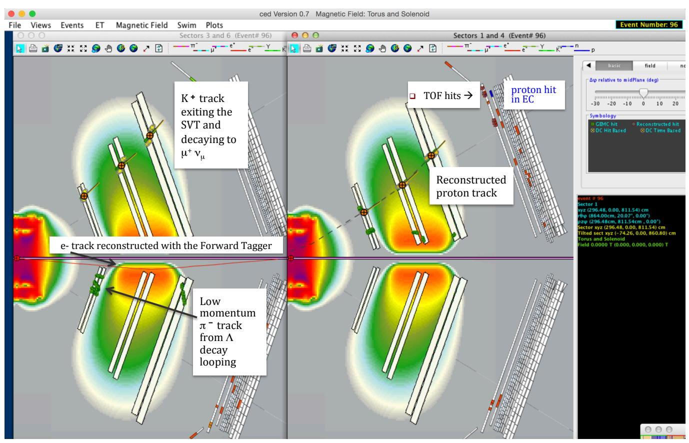

The e- and proton tracks from the reaction $e^- p \rightarrow e^{-\prime} K^+ \Lambda$, $\Lambda \rightarrow p\,\pi^-$ reconstructed in the Forward Detectors

- The filled orange circles correspond to reconstructed 3-D points obtained from pattern recognition; the tangent to the reconstructed track at the 3-D point is represented by the line segment connected to the filled circle.
- The dashed line corresponds to tracks swam to z = 0 with the parameters extracted from the reconstruction algorithm

Figure 30: Event display for the reaction $ep \rightarrow e' K^+ \Lambda$.

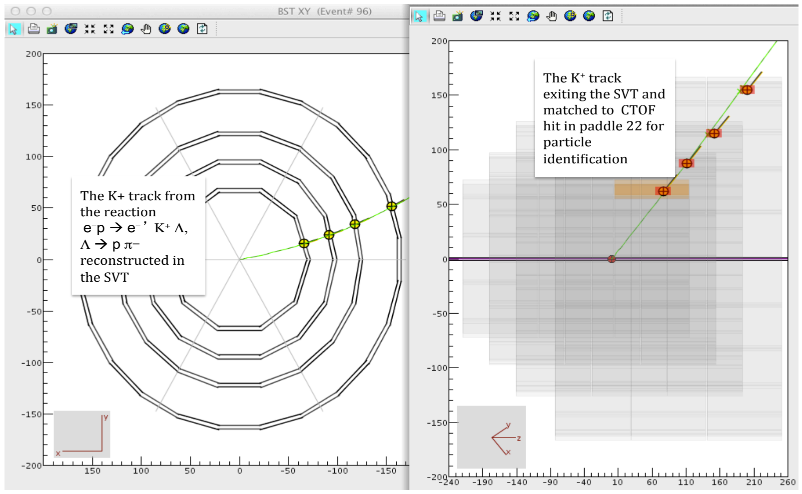

Figure 31: Event display for the reaction $ep \to e'K\Lambda$.

At present, the reconstruction software is still in development. The components that are available are the Silicon Vertex Tracker (SVT), the Central Time of Flight (CTOF), the High Threshold Cherenkov Counter (HTCC), the Drift Chambers (DC), the Forward Time-Of-Flight (FTOF), the Electromagnetic and Pre-shower Calorimeters (EC/PCAL), and the Forward Tagger Calorimeter and Hodoscope. A preliminary version for the Forward MicroMegas Tracker reconstruction is also available and is used to refit the track parameters coming from the DC.

An example of an event for the reaction $ep \to e'K\Lambda$ run through the reconstruction and displayed using the CLAS12 event display CED is shown in Figs. 30 and 31. An overall Event Builder takes the track momentum and flight path information obtained from Central and Forward tracking and links the track to the outer detector to obtain the responses and determine the PID. The electron is mostly identified by the Forward Tagger for the kinematics of the Hybrid Baryon Proposal.

The studies for this letter of intent were done using FastMC. For the Proposal these studies will be repeated by generating events with the event generators described in section IV, tracking all particles through CLAS12 with GEMC and subsequently reconstructing these events with coatjava and obtaining the analysis selection criteria using the kinematic fitter available with the package.

An example of a reconstructed Λ mass spectrum obtained from the missing mass against the eK^+ in the reaction $ep \to e'K^+\Lambda$ generated with GEMC is shown in Fig. 32. The reconstruction uses only the electron detected in the Forward Tagger calorimeter and the produced K^+. Improved mass resolution is obtained when the Λ is reconstructed from the invariant mass of the proton and the π^-.

7.3 Extracting differential cross sections and normalized yields

After the raw data have been subjected to the CLAS12 event reconstruction software package CLARA, we intend to extract differential cross section for all processes with two-body final

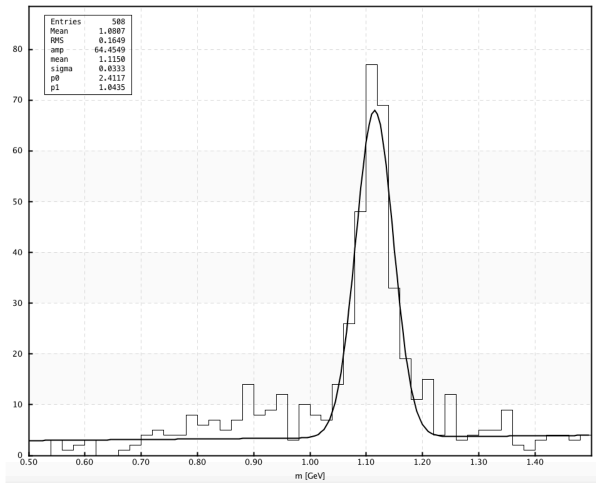

The m.m.(e⁻' K⁺) distribution from the reaction e⁻p → e⁻' K⁺ Λ, Λ → p π− reconstructed using the coatjava package.

Figure 32: Reconstructed Λ mass distribution obtained from the recoil mass against the e' and K^+ for the reaction $ep \to e'K^+\Lambda$ at a beam energy of 6.6 GeV. This figure is obtained using the coatjava plotting package (under development).

states, e.g. KY, $N\pi$, $p\eta$, $p\eta'$, and $p\phi$ using simulations of large amounts of Monte Carlo events to fully understand the acceptances for these processes at the accuracy level required for the partial wave analysis. As for all electroproduction data, the raw cross sections will be subjected to radiative corrections in order to extract the fully corrected differential cross sections. The radiative correction procedure for exclusive processes is well established, and it has been used for correcting single π^+n and $p\pi^\circ$ production as well as $K^+\Lambda$ and $K^+\Sigma$ electroproduction employing the exact procedure developed in Ref. [58]. As it has been recently demonstrated [59], radiative corrections are very important for the analysis of exclusive processes in terms of resonance excitations as they affect both the polar and azimuthal angular dependencies, and consequently the partial wave analyses based on these processes.

For three-body final states, such as $p\pi^+\pi^-$ and $p\eta\pi^\circ$, in addition to extracting differential and integrated cross section, we also we consider event-based analysis techniques, where acceptances will be assigned to each event, and acceptance weighted events will be subjected to a maximum-likelihood fitting procedure. This procedures preserves the full correlations among the final state particles. more on how to separate the different cross sections components: σ_U, σ_{LT} and σ_{TT}

7.4 Partial wave analysis

Using modern partial wave analysis tools several new excited N^* and Δ^* states have been identified or have been significantly improved in their evidence and their star rating in the 2014 edition of the Review of Particle Properties (RPP) of the Particle Data Group [1]. The use of high statistics photoproduction data from CLAS of a number of final states, e.g. $K^+\Lambda$, $K^+\Sigma$, π^+n, $p\pi^\circ$, including polarization observables, was essential in establishing this new evidence. This success has also shown the importance of high statistics data sets in the search for new excited states, and has helped to re-vitalize the field of hadron spectroscopy. In the analysis of the data to be taken with the program discussed in this letter-of-intent, we will make full use of these advanced tools of amplitude and partial wave analysis. Significant progress has also been made in the analysis of electroproduction data where transition form factors have been extracted from several excited states using the high statistics data from CLAS [2, 6, 59]. We expect that these data analysis packages will be well-honed by the time the proposed data will be taken, including the extension of the photoproduction analysis to include the existing and planned electroproduction data sets.

7.5 Analysis of quasi-data to determine CLAS12 sensitivity to minimum detectable resonance elctrocoupling

...

7.6 Threshold values of statitically distinguishable hybrid baryon couplings in $\pi^+\pi^- p$ final state

To estimate threshold values of hybrid state couplings that are distinguishable in data analysis, a phenomenological JM15 [8] model was used. A resonance state with mass M_R = 2.2 GeV, width Γ_R = 200 MeV, and ~~J~~ $J_R = \frac{1}{2}$ was introduced into the model, in addition to the preliminary established contributions from known resonant states as well as non-resonant mechanisms, in the region of W from ~~2.1 to 2.3 GeV~~ $M_R - \Gamma_R/2$ to $M_R + \Gamma_R/2$ and for three Q^2 points (quasi real $Q^2 \approx 0$, 0.65, 1.3 GeV^2).

The statistical significance of hybrid signal was studied at different values of $A_{1/2}$ electrocoupling using a χ^2 criterion. The χ^2 was determined by the following formula (12).

$$\chi^2 = \frac{1}{N_{d.p.}} \sum_{W_i} \sum_{\substack{X=m_{\pi^+\pi^-}, m_{\pi^+p},\\ \theta_{\pi^-}, \alpha_{\pi^-}}} \left(\frac{\left(\frac{d\sigma_{nohyb}}{dX} - \frac{d\sigma_{hyb}}{dX}\right)^2}{\left(\varepsilon_{nohyb}\frac{d\sigma_{nohyb}}{dX}\right)^2 + \left(\varepsilon_{hyb}\frac{d\sigma_{hyb}}{dX}\right)^2} \right) \tag{12}$$

where $m_{\pi^+\pi^-}$, m_{π^+p}, θ_{π^-} and α_{π^-} are the variables that describe the final hadron state. $\frac{d\sigma_{nohyb}}{dX}$ is the single-fold differential cross section with hybrid $A_{1/2} = 0$. $\frac{d\sigma_{nohyb}}{dX}$ is the same cross section with $A_{1/2}$ equal to a certain variable value. ε_{nohyb} and ε_{hyb} are the relative statistical uncertainties of single-fold differential cross sections for the cases when hybrid signal is switched off and on, respectively. The sums run over all points (from 1 to $N_{d.p.}$) of single-fold differential cross sections for all W bins from ~~2.1 to 2.3 GeV~~ $M_R - \Gamma_R/2$ to $M_R + \Gamma_R/2$.

In order to study the threshold values of $A_{1/2}$ electrocoupling for JM model the ~~The~~ statistical uncertainty of single-fold differential cross section with hybrid state was chosen to be the following: 3% at $Q^2 = 1.3$ GeV^2, 2% at $Q^2 = 0.65$ GeV^2, 1% at $Q^2 = 0$ GeV^2. This choice was made, based on the expected reaction yield, roughly estimated in comparison with previous CLAS experiment [50]. ~~Taking into account that the expected DAQ rate in CLAS12 experiments is going to be about ten times higher than in CLAS experiments, run duration is planned to be about two times longer, while the 2π efficiency is expected to be larger~~

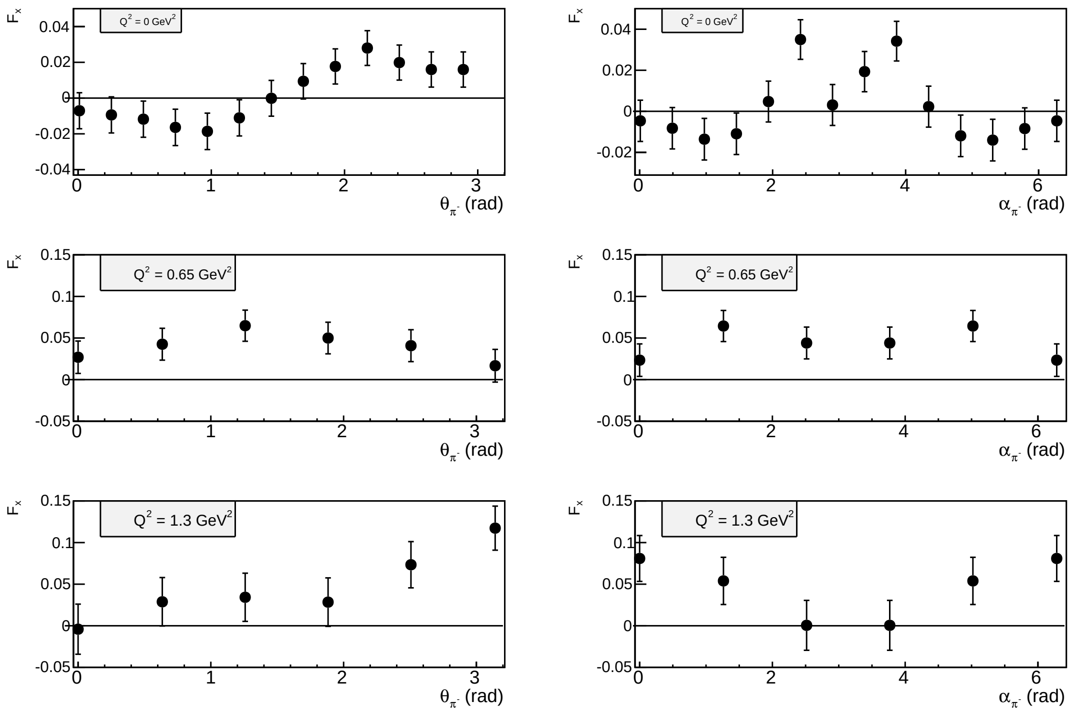

Figure 33: Relative difference between 2π cross sections with and without hybrid state as a function of angles of final hadrons, for three Q^2 points.

Q^2 (GeV)	0.	0.65	1.3
$A_{1/2} \times 10^{-3}$ (GeV$^{-1/2}$)	45	37	19

Table 5: Threshold values of $A_{1/2}$ couplings for statistically distinguishable hybrid state signal.

~~by one order of magnitude.~~, taking into account that in CLAS12 experiments the expected DAQ rate is going to be about ten times higher and the 2π efficiency is also expected to be larger up to one order of magnitude than in CLAS experiments. This choice of uncertainty values also considers the fact that statistics increases with the decrease of photon virtuality.

~~It needs to be mentioned that the aforementioned uncertainty estimation is rather conservative, in the sense that it assumes that just electron trigger will be used. If two or three charged particles trigger will be used a significant increase of 2π events rate is expected and making the statistical uncertainties negligible. Since the KY channel cross section is only few percent of the 2π cross section, run conditions and trigger choice needs to be determined according to KY channel needs.~~

The statistical uncertainty for the single-fold differential cross section without hybrid state (ε_{nohyb}) was assumed to be zero, since in model analysis of real data only experimental data points have errors, while the model cross section is fitted to the data.

The hybrid signal was considered to be statistically significant if $\chi^2 > 4$. The choice of threshold χ^2 value is based on the experience of using JM model for CLAS data fit (see Sect. 3.3). Threshold values of $A_{1/2}$ electrocoupling for statistically significant hybrid state signal are summarized in the Tabl. 5. Obtained threshold values of $A_{1/2}$ electrocoupling for hybrid state do not exceed the electrocouplings values of most of the known resonances in this kinematical region, that makes our estimation very encouraging for the search of new states. ~~If we assume that two or three charged particles trigger is in use, the threshold values of electrocouplings are going to be even lower~~.

The hybrid signal manifests itself mostly in the cross section angular distributions. In Fig. 33 the relative difference of 2π cross section with and without hybrid state are plotted as functions of θ_{π^-} and α_{π^-} angles for three Q^2 bins. Distributions in Fig. 33 are produced for the threshold values of $A_{1/2}$ electrocoupling listed in Tabl. 5. As it is seen from the plots in Fig. 33, this difference grows as Q^2 increases, that corresponds to the fact that relative contribution of resonant part to the total 2π cross section increases with Q^2.

Ability of the model to distinguesh the new state highly depends on data statistics. For instance if the requested beam time would be two times smaller than the minimum distingueshable $A_{1/2}$ electrocoupling will increase up to 65 at Q^2 close to zero, that inevitably weakens the sensitivity of this approach to the new states manifestation.

7.7 Threshold values of statistically distinguishable hybrid baryons electrocouplings from $K\Lambda$ final state

In order to quantify the statistical significance of the difference between the exclusive KY event distributions over the θ_K, ϕ_K CMS angles, simulated according to the models A and B, as described in paragraph 3.4, the following χ^2 definition has been be used:

$$\chi^2 = \frac{1}{N_{d.p.}} \sum_{W,cos(\theta_K),\phi_K} \frac{\left(\frac{d^2\sigma_A}{d\Omega_K} - \frac{d^2\sigma_B}{d\Omega_K}\right)^2}{\delta^2}, \tag{13}$$

where $\frac{d^2\sigma_A}{d\Omega_K}$ and $\frac{d^2\sigma_B}{d\Omega_K}$ are the cross sections simulated in the models A and B, respectively.

The χ^2 is evaluated in each Q^2 bin independently and we choose a 0.1 GeV^2 bin width in Q^2. The sum over W in (13) runs from $M_R - \Gamma_R/2$ to $M_R + \Gamma_R/2$ and the bin width in W is 20 MeV. We used 24 bins in $cos(\theta_K)$ and ϕ_K. Assuming that the statistical uncertainties dominate, the uncertainties for the differences $\left(\frac{d^2\sigma_A}{d\Omega_K} - \frac{d^2\sigma_B}{d\Omega_K}\right)$ between the event distributions simulated in the models B and A, respectively, can be evaluated as:

$$\delta^2 = \left(\frac{\frac{d^2\sigma_A}{d\Omega_K}}{\sqrt{N_A}}\right)^2 + \left(\frac{\frac{d^2\sigma_B}{d\Omega_K}}{\sqrt{N_B}}\right)^2, \tag{14}$$

where N_A and N_B are the number of events in three dimensional bins in W and Ω_K for the two models.

The number of events in the mentioned above three dimensional bins for a given Q^2 bin can be calculated knowing the expected total number of events in the whole covered kinematic space. The number of events in each multidimensional bin is proportional to the cross section in that bin, taking acceptance into account. The cross section $\frac{d^2\sigma}{d\Omega_K}$ are obtained by integrating over the other kinematic variables: final state electron azimuthal angle ϕ_e and spherical angles of one of the Λ decay product particles, say proton, θ_p, ϕ_p, assuming that the cross section $\frac{d^5\sigma}{d\Omega_K d\phi_e d\theta_p d\phi_p}$ does not depend on ϕ_e, θ_p and ϕ_p. Then the number of events (N) in every four dimensional bin is

$$N(Q^2, W, \theta_K, \phi_K) = C \int_{\phi_e,\theta_p,\phi_p} a\times \frac{d^5\sigma}{d\theta_K d\phi_K d\phi_e d\theta_p d\phi_p} = C \int_{\phi_e,\theta_p,\phi_p} a\times \frac{d^2\sigma}{d\Omega_K} \approx C \sum_{\phi_e,\theta_p,\phi_p} a\times \frac{d^2\sigma}{d\Omega_K}, \tag{15}$$

where a is the CLAS12 acceptance, which depends on all kinematic variables and C is a constant. Set the sum of all $N(Q^2, W, \theta_K, \phi_K)$ equal to the expected total number of events in the whole kinematic covered space we find the constant C.

The number of evens in each multidifferential bin was calculated assuming the total number of $K\Lambda$ events to be collected in the experiment is 2×10^8 (see section 6.4).

The typical number of events in one bin of the single differential distribution $\frac{d\sigma}{dcos(\theta_K)}$ is about few thousands and the statistical errors are negligible, while in two fold differential distribution $\frac{d^2\sigma}{d\Omega_K}$ statistical errors are meaning. This can be seen in Figs. 34 through 37

We define the the minimal value of the photocoupling such as it is the minimal value of the photocoupling when the χ^2 from (13) characterizing the difference between two cross sections is more than 4. The minimal values of A_{12}, A_{32} and S_{12} found in this way are presented in Tables 6 and 7. The mass of the hybrid state was 2.2 GeV and the total width was 0.250 GeV. The Q^2 bin width was 0.1 GeV^2.

Table 6: The minimal values of the photocouplings for the beam energy 6.6 GeV and the torus current -2950 A for the resonances with the spin (J_R) 1/2 and 3/2. A_{12}, A_{32} and S_{12} are in the units of $10^{-3}\times$GeV$^{-1/2}$. When determining the minimal value of A_{12} we varied only A_{12} setting the other photocouplings to zero. The minimal values of A_{32} and S_{12} were obtained in the same way.

Q^2, GeV^2	J_R=1/2		J_R=3/2		
	A_{12}	S_{12}	A_{12}	A_{32}	S_{12}
0.1	12	12	16	11	10
0.5	17	19	18	19	12
1.0	16	21	16	18	10

It was found that the minimal photocoupling values are weakly dependent on the run conditions and Q^2. The weak dependence on Q^2 can be explained. The resonance manifestation is more pronounced at small Q^2, as the non-resonant background is smaller, on the other hand statistical errors are larger (the same Q^2 bin width (0.1 GeV^2) is used at all Q^2) and the sensitivity to the resonance gets smaller. These two factor works in opposite direction and the χ^2 does not change significantly.

Figs. 34 through 37 present examples of the comparison of the model to the model plus resonance one- and two fold differential cross sections. The model plus resonance cross section was calculated when the photocoupling was set to its minimal value from the Table 7.

Table 7: The minimal values of the photocouplings for the beam energy 8.8 GeV and the torus current -2950 A for the resonances with the spin (J_R) 1/2 and 3/2. A_{12}, A_{32} and S_{12} are in the units of $10^{-3}\times\mathrm{GeV}^{-1/2}$. When determining the minimal value of A_{12} we varied only A_{12} setting the other photocouplings to zero. The minimal values of A_{32} and S_{12} were obtained in the same way.

Q^2, GeV^2	J_R=1/2		J_R=3/2		
	A_{12}	S_{12}	A_{12}	A_{32}	S_{12}
0.3	12	12	14	12	9
0.5	19	20	19	21	12
1.0	16	21	16	18	9

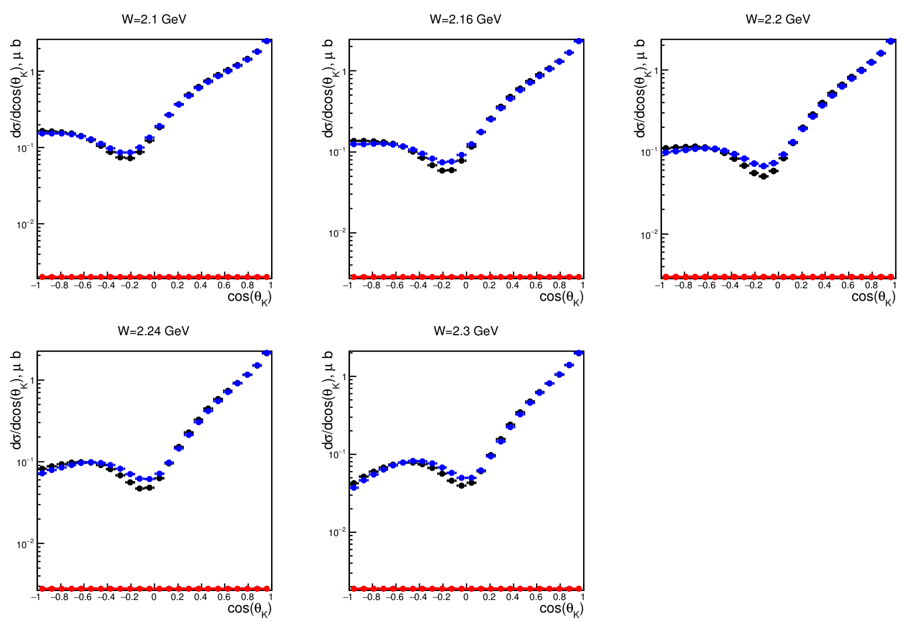

Figure 34: Comparison of the model cross section $d\sigma/d\cos(\theta_K)$ (black points) with the model plus resonance cross section (blue points) for the beam energy 8.8 GeV and the torus current -2950 A at Q^2=0.3 GeV^2 and at few values of W. The cross section of the resonance contribution is shown in red. The spin of the resonance is 1/2 and the A_{12} is $12\times10^{-3}\mathrm{GeV}^{-1/2}$, it corresponds to the minimal A_{12} from the table 7. Statistical errors are negligible.

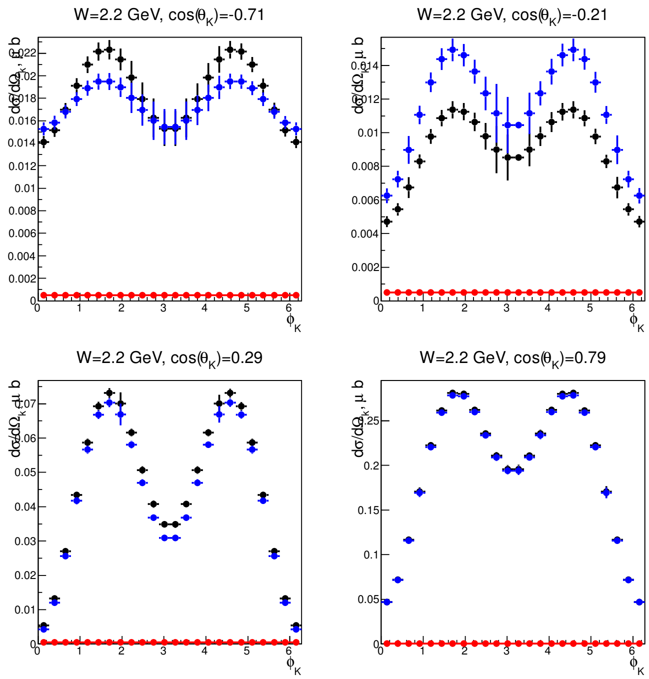

Figure 35: Comparison of the model cross section $d\sigma/d\Omega(\theta_K)$ with the model plus resonance cross section at $W = M_R$ and few values of $cos(\theta_K)$. The same conditions run condition and Q^2 as in Fig. 34. The errors are statistical only.

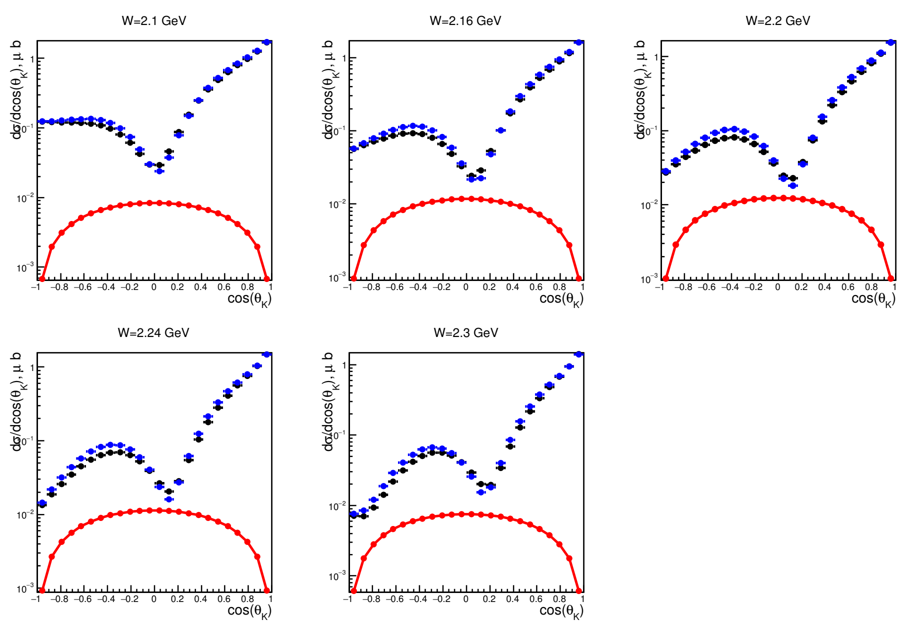

Figure 36: Comparison of the model cross section $d\sigma/d\cos(\theta_K)$ (black points) with the model plus resonance cross section (blue points) for the beam energy 8.8 GeV and the torus current -2950 A at Q^2=0.3 GeV^2 and at few values of W. The cross section of the resonance contribution is shown in red. The spin of the resonance is 3/2 and the A_{32} is $18{\times}10^{-3}$GeV$^{-1/2}$, it corresponds to the minimal A_{32} from the table 7. Statistical errors are negligible.

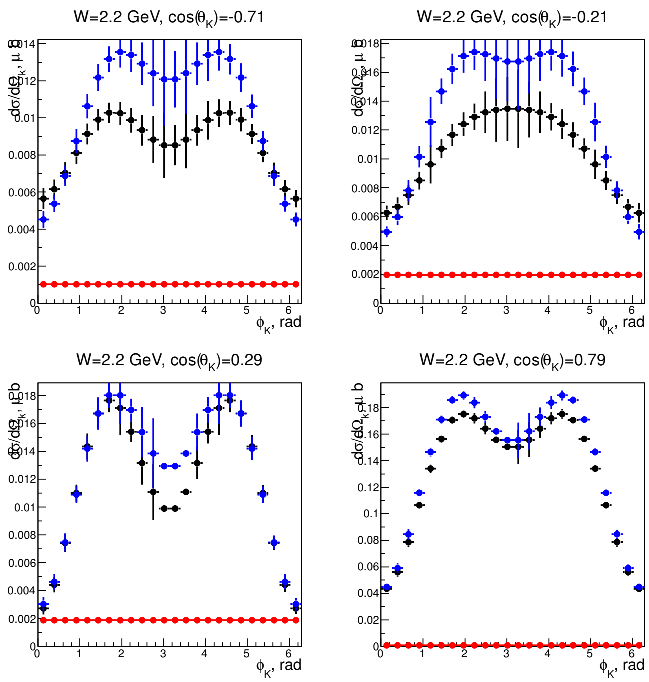

Figure 37: Comparison of the model cross section $d\sigma/d\Omega(\theta_K)$ with the model plus resonance cross section at $W = M_R$ and few values of $cos(\theta_K)$. The same conditions run condition and Q^2 as in Fig. 36. The errors are statistical.

7.8 Experimental sensitivity to hybrid resonance states in $\pi + \pi^- p$ and KY final states

The ability of JM model to distinguish hybrid state signal is also illustrated in Fig. 38, where the χ^2 value is plotted as a function of the resonance mass for three Q^2 points and various values of $A_{1/2}$ electrocoupling. The dip in χ^2 dependences is clearly seen on the W_h value corresponding to the expected mass of the hybrid state when $A_{1/2}$ electrocoupling value exceeds threshold.

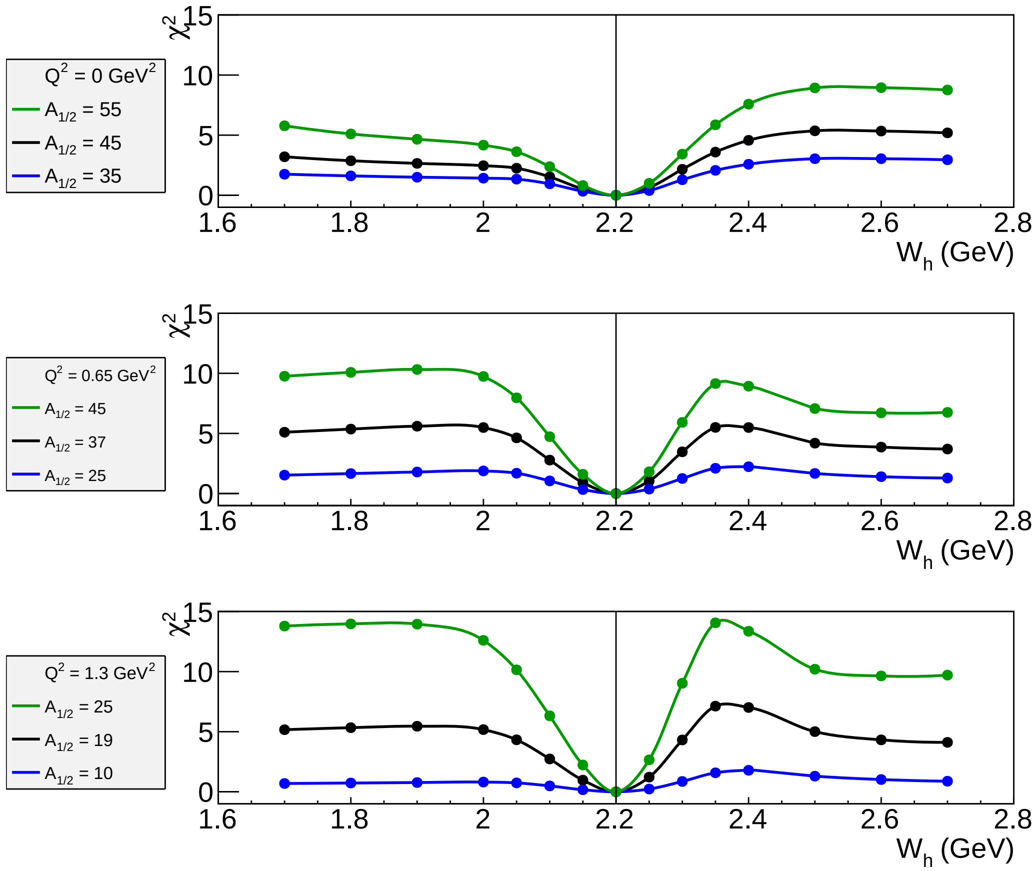

Figure 38: χ^2 versus W_h distributions for three Q^2 values (0 GeV^2, 0.65 GeV^2, 1.3 GeV^2) obtained from JM model. For each value of Q^2 the distributions were plotted for three values of $A_{1/2}$ electrocoupling (see legend for each plot).

8 Beamtime estimate

The complete hybrid baryon program will require 2 beam energies, 6.6 GeV, 8.8 GeV to cover with high statistics the lowest Q^2 range where the scattered electron is detected in the angle range from $2.5° \leq \theta_e \leq 4.5°$. We request new beam time of 60 days that are divided into 30 days at 6.6 GeV and 30 days at 8.8 GeV.

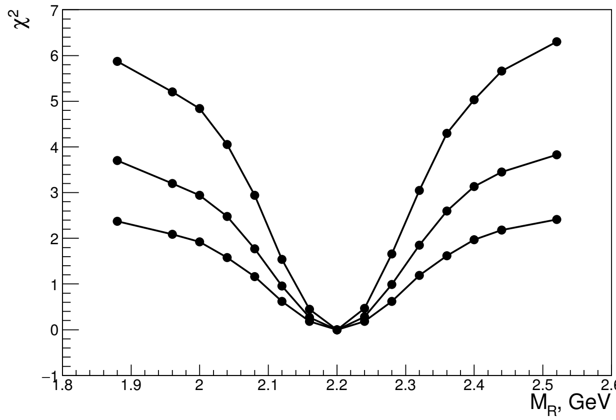

Figure 39: The χ^2 between two model cross sections. One cross section was calculated with the hybrid mass equal to 2.2 GeV. The other cross section was calculated with the variable hybrid mass (M_R). The χ^2 square was calculated as described in section **??** using the estimated statistical errors. Three lines from bottom to top correspond to the three values of A_{12}: 15, 19 and 25 in the units of 10^{-3} GeV$^{-1/2}$. The value 19 is the minimal A_{12} from the table 7 for the spin 1/2 resonance at Q^2=0.5 GeV^2. Run condition are as in the same table.

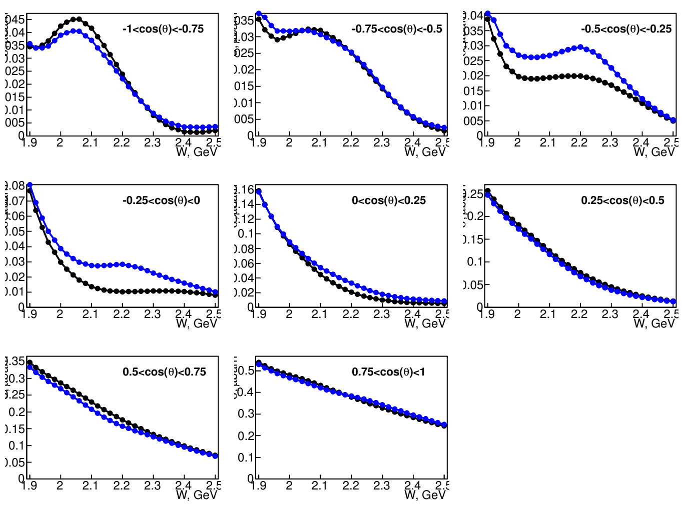

Figure 40: The integrated model cross section (in black) and model plus resonance (A_{12}=40×10^{-3} GeV$^{-1/2}$) cross section (in blue) at different $cos(\theta_K)$ bins and at Q^2=0.5 GeV^2. The pronounced structures at small $cos(\theta_K)$ can be idications of a resonance.

9 Summary

In this Proposal we laid out an extensive program to study the excitation of nucleon resonances in meson electroproduction using electron beam energies of 6.6 and 8.8 GeV. The main focus is on the search for gluonic light-quark baryons in the mass range up to 3.0 GeV and in the Q^2 range from 0.05 to 2.0 GeV^2. We have estimated the rates for two of the channels we propose to study, $K^+\Lambda$ ($K^+\Sigma$) and $p\pi^+\pi^-$, but all other channels detected in CLAS12 will be subjected to analyses as well. The expected rates are very high, thanks to the very forward scattered electrons with a minimum Q^2 of 0.05 GeV^2 that are detected in the Forward Tagger. The data will be subjected to state-of-the-art partial wave analyses that were developed during the past years for baryon resonance analyses. Beyond the main focus of this Proposal on hybrid baryons, a wealth of data will be collected in many different channels that will put meson electroproduction data on par with real photoproduction in terms of production rates and will allow for a vast extension of the ongoing N^* electroexcitation program with CLAS at lower energies. It will complement the already approved program to study nucleon resonance excitations at the highest Q^2 achievable at 11 GeV beam energy, by the experiment E12-11-005.

A Appendix A - KY electroproduction

The electroproduction of KY on the proton may be described as follows. To be reviewed and completed

The exclusive reaction cross sections for photon absorption by the proton $\frac{d^2\sigma}{d\Omega_K}$ can be determined in the single photon exchange approximation based on the conventions for the production amplitudes explained in [60]. These cross sections are related to the measured exclusive electron scattering cross sections $\frac{d^4\sigma}{dW dQ^2 d\Omega_K}$ by:

$$\frac{d^4\sigma}{dW dQ^2 d\Omega_K} = \Gamma_v \frac{d^2\sigma}{d\Omega_K}, \tag{16}$$

where Γ_v is the virtual photon flux defined by the momenta of the incoming and outgoing electrons:

$$\Gamma_v = \frac{\alpha}{4\pi}\frac{1}{E_b^2 M_p^2}\frac{W(W^2 - M_p^2)}{(1-\varepsilon)Q^2} \ , \tag{17}$$

and α is the fine structure constant, E_b is the beam energy, M_p is the proton mass, and ε is the virtual photon transverse polarization given by

$$\varepsilon = \left(1 + 2\left(1 + \frac{\nu^2}{Q^2}\right)\tan^2\left(\frac{\theta_{\mathrm{e}}}{2}\right)\right)^{-1} \ , \tag{18}$$

where ν is the virtual photon energy, θ_e is the electron scattering angle in the laboratory frame, and $d\Omega_K$ the element of the solid angle of kaon emission in the CMS frame.

Alternatively, the exclusive electron scattering cross sections off protons $\frac{d^5\sigma}{dE' d\Omega_{e'} d\Omega_K}$ can be obtained employing another set of variables for the scattered electron, where $dE^{'}$ and $d\Omega_{e'}$ represent the differentials for energy and solid angle of the scattered electron in the lab frame:

$$\begin{aligned} \frac{d^5\sigma}{dE' d\Omega_{e'} d\Omega_K} &= \Gamma_v^{'} \frac{d^2\sigma}{d\Omega_K}, \\ \Gamma_v^{'} &= \frac{\alpha}{2\pi^2}\frac{E_{e'}}{E_b}\frac{(W^2 - M_p^2)}{(1-\varepsilon)2M_p Q^2} \ . \end{aligned} \tag{19}$$

The formalism that relates the amplitude for exclusive hadron electroproduction off protons to the measurable cross sections is described in details in [62]. Here we outline the part of this formalism which is relevant to the studies proposed in the LOI. The two-fold differential cross section $\frac{d^2\sigma}{d\Omega_K}$ for KY electroproduction off the protons can be computed as a contraction of leptonic and hadronic tensors divided by the invariant virtual photon flux and multiplied by the phase space differential for the two-body final state $d^2\Phi$:

$$d^2\Phi = \frac{q_K d\Omega_K}{4\pi^2 4W}, \tag{20}$$

where q_K is the absolute value of the kaon three momentum in the CMS frame. The leptonic tensor $L_{\mu\nu}$ is well known from QED [62]. The hadronic tensor $W_{\mu\nu}$ represents a product of the hadronic currents J^*_μ and J_ν contracted with the spin-density matrices for the initial and the final hadrons $\rho_{\lambda_{p'},\lambda_p}$, $\rho_{\lambda_{f'},\lambda_f}$:

$$W_{\mu\nu} = \sum_{\lambda_{p'},\lambda_p,\lambda_{f'},\lambda_f} J^*_\mu(\lambda_{p'},\lambda_{f'})J_\nu(\lambda_p,\lambda_f)\rho_{\lambda_{p'},\lambda_p}\rho_{\lambda_{f'},\lambda_f}, \tag{21}$$

where $\lambda_{p'}$,λ_p, and $\lambda_{f'}$, λ_f stand for the helicities of the initial proton and for the helicities of the final hadrons, respectively. The sum is running over repetitive indices. In a case of an unpolarized initial proton and unpolarized final hadrons, the density matrices can be written as:

$$\begin{aligned} \rho_{\lambda_{p'},\lambda_p} &= \frac{1}{2}I \text{ , and} \\ \rho_{\lambda_{f'},\lambda_f} &= I, \end{aligned} \tag{22}$$

where I is the unity matrix.

Contracting the leptonic [62] and hadronic (21) tensors in the lab frame, we obtain the following expression for two-fold differential KY cross section $\frac{d\sigma}{d\Omega_K}$:

$$\begin{aligned} \frac{d\sigma}{d\Omega_K} &= \frac{4\pi\alpha}{4K_LM_N}[\frac{J^*_xJ_x+J^*_yJ_y}{2}+\epsilon_LJ^*_zJ_z \\ +\epsilon_T\frac{J^*_xJ_x-J^*_yJ_y}{2} &- \sqrt{2\epsilon_L(1+\epsilon_T)}\frac{J^*_xJ_z+J^*_zJ_x}{2}]\frac{q_K}{4\pi^2 4W}, \end{aligned} \tag{23}$$

where α is fine structure constant and ϵ_L stands for degree of longitudinal polarization of virtual photons. QED gives for ϵ_L[62]:

$$\epsilon_L = \sqrt{\frac{Q^2}{\nu^2}}\epsilon. \tag{24}$$

The factor $4K_LM_N$ is the invariant virtual photon flux with M_N is nucleon mass and K_L is the equivalent photon energy:

$$K_L = \frac{W^2-M_N^2}{2M_N}. \tag{25}$$

The four terms in (23) generate four structure functions that define the exclusive electroproduction cross section, transverse (T), longitudinal (L), and two interference structure functions transverse-transverse (TT) and transverse-longitudinal (TL):

$$\frac{d\sigma}{d\Omega_K} = \frac{d\sigma_T}{d\Omega_K} + \epsilon_L\frac{d\sigma_L}{d\Omega_K} + \epsilon_T\frac{d\sigma_{TT}}{d\Omega_K}cos(2\phi_K) + \sqrt{2\epsilon_L(1+\epsilon_T)}\frac{d\sigma_{TL}}{d\Omega_K}cos(\phi_K). \tag{26}$$

After integration of the two-fold differential cross section (23, 26) $d^2\sigma/d\Omega_K$ over the azimuthal ϕ_K angle of the final K, all interference structure functions disappear and the (23, 26) are reduced to the simpler expressions:

$$\frac{d\sigma}{d(-cos(\theta_K))} = \frac{4\pi\alpha}{4K_LM_N}\left\{\frac{J^*_xJ_x+J^*_yJ_y}{2}+\epsilon_LJ^*_zJ_z\right\}\frac{q_K}{2\pi 4W}, \tag{27}$$

and

$$\frac{d\sigma}{d(-cos(\theta_K))} = \frac{d\sigma_T}{d(-cos(\theta_K))} + \epsilon_L \frac{d\sigma_L}{d(-cos(\theta_K))}. \tag{28}$$

The hadronic current J_ν in the lab frame is related to reaction helicity amplitudes [60]:

$$J_x = -\frac{\langle \lambda_f|T|\lambda_p\lambda_\gamma = 1\rangle - \langle \lambda_f|T|\lambda_p\lambda_\gamma = -1\rangle}{\sqrt{2}},$$
$$J_y = i\frac{\langle \lambda_f|T|\lambda_p\lambda_\gamma = 1\rangle + \langle \lambda_f|T|\lambda_p\lambda_\gamma = -1\rangle}{\sqrt{2}}, \text{ and}$$
$$J_z = \frac{\nu}{\sqrt{Q^2}}\langle \lambda_f|T|\lambda_p\lambda_\gamma = 0\rangle. \tag{29}$$

The J_0 component of the hadronic current is determined by the current conservation:

$$q_0 J^0 - q_z J^z = 0. \tag{30}$$

B Appendix B - Hybrid Baryon excitation Amplitude

to be checked and completed

The hadronic decay amplitudes $\langle \lambda_f|T_{dec}|\lambda_R\rangle$ are related to the Γ_{λ_f} partial hadronic decay widths of the N^* to KY final states f of helicity $\lambda_f = \lambda_Y$ by:

$$\langle \lambda_f|T_{dec}|\lambda_R\rangle = \langle \lambda_f|T^{J_r}_{dec}|\lambda_R\rangle d^{J_r}_{\mu\nu}(\cos\theta_K)e^{i\mu\phi_K},$$

with $\mu = \lambda_R$ and $\nu = -\lambda_Y$, and

$$\langle \lambda_f|T^{J_r}_{dec}|\lambda_R\rangle = \frac{2\sqrt{2\pi}\sqrt{2J_r+1}M_r\sqrt{\Gamma_{\lambda_f}}}{\sqrt{p^r_i}}\sqrt{\frac{p^r}{p}}. \tag{31}$$

p^r and p are the magnitudes of the three-momenta of the final state K for the $N^* \to KY$ decay evaluated at $W = M_r$ and at the running W, respectively. The variables θ_K, ϕ_K are the CMS polar and azimuthal angles for the final kaon, and J_r stands for the N^* spin.

The final state Λ or Σ baryons can only be in the helicity states $\lambda_f = \pm\frac{1}{2}$. The hadronic decay amplitudes $\langle \lambda_f|T^{J_r}_{dec}|\lambda_R\rangle$ with $\lambda_f = \pm\frac{1}{2}$ are related by P-invariance, which imposes the absolute values for both amplitudes to be the same. Therefore, the hybrid state partial decay widths to the $K\Lambda$ and $K\Sigma$ final states Γ_{λ_f} can be estimated as:

$$\Gamma_{\lambda_f} = \frac{1}{2}\Gamma_r 0.03, \tag{32}$$

where the factor 0.03 reflects the adopted 3% BF for hybrid baryon decays to the KY final state.

The following relationships between the transition amplitudes $\langle \lambda_R | T_{em} | \lambda_\gamma \lambda_p \rangle$ and the $\gamma_v NN^*$ electrocouplings from [51] have been used:

$$\begin{aligned}
\langle \lambda_R | T_{em} | \lambda_\gamma \lambda_p \rangle &= \frac{W}{M_r} \sqrt{\frac{8 M_N M_r q_{\gamma_r}}{4\pi\alpha}} \sqrt{\frac{q_{\gamma_r}}{q_\gamma}} A_{1/2,3/2}(Q^2), \\
\text{with } |\lambda_\gamma - \lambda_p| &= \frac{1}{2}, \frac{3}{2} \text{ for transverse photons, and} \\
\langle \lambda_R | T_{em} | \lambda_\gamma \lambda_p \rangle &= \frac{W}{M_r} \sqrt{\frac{16 M_N M_r q_{\gamma_r}}{4\pi\alpha}} \sqrt{\frac{q_{\gamma_r}}{q_\gamma}} S_{1/2}(Q^2), \\
&\text{for longitudinal photons,}
\end{aligned} \tag{33}$$

where q_γ is the absolute value of the initial photon three-momentum of virtuality $Q^2 > 0$ with $q_\gamma = \sqrt{Q^2 + E_\gamma^2}$ and E_γ the photon energy in the CMS frame at the running W

$$E_\gamma = \frac{W^2 - Q^2 - M_N^2}{2W}. \tag{34}$$

The $q_{\gamma,r}$ value is then computed from (34) with W=M_r.

References

[1] K. A. Olive *et al.* [Particle Data Group Collaboration], Chin. Phys. C **38**, 090001 (2014)

[2] I. G. Aznauryan and V. D. Burkert, Prog. Part. Nucl. Phys. **67**, 1 (2012).

[3] I.G. Aznauryan *et al.*, Int. J. Mod. Phys. E **22**, 1330015 (2013).

[4] I. G. Aznauryan *et al.* [CLAS Collaboration], Phys. Rev. C **78**, 045209 (2008).

[5] T. Barnes and F. E. Close, Phys. Lett. B **123**, 89 (1983); E. Golowich, E. Haqq, and G. Karl, Phys. Rev. D **28**, 160 (1983); C.E. Carlson and T.H. Hansson, Phys. Lett. B **128**, 95 (1983); I. Duck and E. Umland, Phys. Lett. B **128** (1983) 221.

[6] I. G. Aznauryan *et al.* [CLAS Collaboration], Phys. Rev. C **80**, 055203 (2009).

[7] J. J. Dudek and R. G. Edwards, Phys. Rev. D **85**, 054016 (2012).

[8] V. I. Mokeev, V. D. Burkert, T. S. H. Lee, L. Elouadrhiri, G. V. Fedotov and B. S. Ishkhanov, Phys. Rev. C **80**, 045212 (2009).

[9] L. De Cruz, J. Ryckebusch, T. Vrancx and P. Vancraeyveld, Phys. Rev. C **86**, 015212 (2012).

[10] A. Anisovich *et al.*, Eur. Phys. J. A **48**, 15 (2012).

[11] D. Ronchen *et al.*, Eur. Phys. J. A **50**, 101 (2014).

[12] A.P. Szczepaniak and M.R. Pennington, Phys. Lett. B **737**, 283 (2014).

[13] See http://pdg.lbl.gov/2015/reviews/rpp2015-rev-n-delta-resonances.pdf

[14] S. Capstick and P. R. Page, Phys. Rev. C **66**, 065204 (2002); Phys. Rev. D **60**, 111501 (1999).

[15] P. R. Page, Int. J. Mod. Phys. A **20**, 1791 (2005).

[16] C. K. Chow, D. Pirjol and T. M. Yan, Phys. Rev. D **59**, 056002 (1999).

[17] C. E. Carlson and N. C. Mukhopadhyay, Phys. Rev. Lett. **67**, 3745 (1991).

[18] T. T. Takahashi and H. Suganuma, Phys. Rev. Lett. **90**, 182001 (2003).

[19] E. Kou, Phys. Rev. D **63**, 054027 (2001).

[20] Z. P. Li, Phys. Rev. D **44**, 2841 (1991).

[21] Z. P. Li, V. Burkert and Z. J. Li, Phys. Rev. D **46**, 70 (1992).

[22] T. Vrancx, J. Ryckebusch and J. Nys, Phys. Rev. C **89**, no. 6, 065202 (2014)

[23] The StrangeCalc web-site http://rprmodel.ugent.be/calc/

[24] I. V. Anikin, V. M. Braun, and N. Offen, Phys. Rev. D **92**, 074044 (2015).

[25] J. Segovia , B. El-Bennich, E. Rojas, et al., Phys. Rev. Lett. **115**, 015203 (2015).

[26] V. I. Mokeev et al., Phys. Rev. C **93**, 054016 (2016).

[27] M. Dugger et al., (CLAS Collaboration), Phys. Rev. C **79**, 065206 (2009).

[28] K. Park et al., (CLAS Collaboration), Phys. Rev. C **91**, 045203 (2015).

[29] V. I. Mokeev et al., Eur. Phys. J. Web Conf. **113**, 01013 (2016).

[30] A. V. Anisovich et al., Eur. Phys. J. A **48**, 15 (2012).

[31] A. V. Anisovich et al., Eur. Phys. J. A **48**, 88 (2012).

[32] A. V. Anisovich et al., Eur. Phys. J. A **49**, 158 (2013).

[33] J. W. C. McNabb et al. (CLAS Collaboration), Phys. Rev. C **69**, 042201 (2004).

[34] R. Bradford et al. (CLAS Collaboration), Phys. Rev. C **73**, 035202 (2006).

[35] R. Bradford et al. (CLAS Collaboration), Phys. Rev. C **75**, 035205 (2007).

[36] M. E. McCracken et al. (CLAS Collaboration), Phys. Rev. C **81**, 025201 (2010).

[37] K. H. Glander et al. (SAPHIR Collaboration), Eur. Phys. J. A **19**, 251 (2004).

[38] T. C. Jude et al. (Crystal Ball Collaboration), Phys. Lett. B **735**, 035205 (2014).

[39] A. Lleres et al. (GRAAL Collaboration), Eur. Phys. J. A **31**, 79 (2007).

[40] A. Lleres et al. (GRAAL Collaboration), Eur. Phys. J. A **39**, 149 (2009).

[41] A. Sarantsev, "The BoGa Amplitude Analysis Methods and its Extension to High W and to Electroproduction", the invited talk at the Workshop "Nucleon Resonances: From Photoproduction to High Photon Virtualities", ECT*, Trento, October 12-16 2015, http:/boson.physics.sc.edu gothe/ect*-15program.html

[42] H. Kamano, S. X. Nakamura, T-S. H. Lee, T. Sato, Phys. Rev. C **88**, 035209 (2013).

[43] H. Kamano, T-S. H. Lee, AIP Conf. Proc. **1432**, 74 (2012).

[44] N. Suzuki,T. Sato, and T-S. H. Lee, Phys. Rev. C **82**, 045206 (2010).

[45] J. Nys, "Hunting the Resonances in $p(\gamma, K^+)\Lambda$ Reactions: (Over)Complete Measurements and Partial-Wave Analyses", the invited talk at the Workshop "Nucleon Resonances: From Photoproduction to High Photon Virtualities", ECT*, Trento, October 12-16 2015, http:/boson.physics.sc.edu gothe/ect*-15program.html

[46] M. Ripani, V. Mokeev, M. Anghinolfi, M. Battaglieri, G. Fedotov, E. Golovach, B. Ishkhanov and M. Osipenko *et al.*, Nucl. Phys. A **672**, 220 (2000).

[47] I. G. Aznauryan, V. D. Burkert, G. V. Fedotov, B. S. Ishkhanov and V. I. Mokeev, Phys. Rev. C **72**, 045201 (2005).

[48] V. I. Mokeev et al., in "Proc. of the Workshop on the Physics of Excited Nucleon. NSTAR2005", ed. by S. Capstick, V. Crede, P. Eugenio, World Scientific Publishing Co., p. 47.

[49] For details see: https://www.jlab.org/Hall-B/clas12-web/

[50] M. Ripani *et al.* [CLAS Collaboration], Phys. Rev. Lett. **91**, 022002 (2003)

[51] V. I. Mokeev *et al.* [CLAS Collaboration], Phys. Rev. C **86**, 035203 (2012)

[52] G. V. Fedotov *et al.* [CLAS Collaboration], Phys. Rev. C **79**, 015204 (2009)

[53] C. Wu, J. Barth, W. Braun, J. Ernst, K. H. Glander, J. Hannappel, N. Jopen and H. Kalinowsky *et al.*, Eur. Phys. J. A **23**, 317 (2005).

[54] Aachen-Berlin-Bonn-Hamburg-Heidelberg-Munich Collaboration, Phys. Rev. **175**, 1669-1696 (1968).

[55] E. Golovach et al., $\gamma p \rightarrow p\pi^+\pi^-$ cross sections from g11a experiment, CLAS ANALYSIS NOTE (in preparation).

[56] Mo, Luke W. and Tsai, Yung-Su Rev. Mod. Phys. **41**, 205-235 (1969).

[57] T. Corthals, D. G. Ireland, T. Van Cauteren and J. Ryckebusch, Phys. Rev. C **75**, 045204 (2007).

[58] A. Afanasev, I. Akushevich, V. Burkert and K. Joo, Phys. Rev. D **66**, 074004 (2002).

[59] K. Park *et al.* [CLAS Collaboration], Phys. Rev. C **91**, 045203 (2015).

[60] V. I. Mokeev et. al., Phys. Rev. C **80**, 022002 (2009).

[61] D. Luke and P. Soding, Multiple Pion Photoproduction in the s Channel Resonance Region, Springer Tracts in Modern Physics 59 (1971).

[62] E. Amaldi, S. Fubini and G. Furlan, Pion Electroproduction. Springer Tracts in Modern Physics **83**, ed. by G. Hohler (Springer Verlag, Berlin 1979).